Development of Gold Nanocluster-Based Biosensors

Xinzhe Zhou

Thesis submitted to the faculty of the Virginia Polytechnic Institute and State University
in partial fulfillment of the requirements for the degree of

Master of Science
In
Civil Engineering

Linsey C. Marr, Chair
Peter Vikesland
Amy Pruden

September 3, 2015
Blacksburg, VA

Keywords: Gold Nanoclusters, Density Gradient Centrifugation, Surface-Enhanced Raman Scattering, Influenza Virus, Aptamer, Biosensor

Development of Gold Nanocluster-Based Biosensors

Xinzhe Zhou

ABSTRACT

Gold nanoclusters possess both theoretical and practical importance in the development of ultrasensitive biosensors based on surface-enhanced Raman spectroscopy (SERS). Manipulation of gold nanoclusters in a predictable and reproducible manner for the application of refined biochemical analysis still remains challenging. In this study, high-purity gold nanoclusters are isolated via a simple method based on density gradient centrifugation. Three distinct bands including monomers, small aggregates (2-4 nanospheres), and large aggregates (>5 nanospheres) can be separated via density gradient centrifugation. The isolated gold nanoclusters greatly enhance the Raman intensity of the trapped dye molecules such that single nanocluster detection is feasible. To develop a gold nanoparticle-based biosensor for influenza virus, effort was also made to modify recognition moieties such as aptamers to gold nanoparticles via distinct approaches. The increase of hydraulic diameter and the shift of optical absorbance spectrum indicate the success of surface modification to gold nanoparticles.

ACKNOWLEDGEMENTS

I would like to thank my advisor, Linsey C. Marr, for her knowledgeable, inspiring, and experienced instructions on how to pursue challenging goals. Keeping humble and approaching step by step is the research philosophy I learned from Linsey. Meanwhile, her encouragement and inspiration have driven me to keep enthusiastic and confident to conquer every obstacle in my research. I would also like to thank the other members of my committee, Dr. Peter Vikesland and Dr. Amy Pruden. Their professional insight in nanotechnology and microorganism is indispensable in building up my research projects. I am grateful to Dr. Elankumaran Subbiah, Dr. Tijana Grove for their kind help to clarify my long-lasting dilemma in research.

I am extremely thankful to my fellow researchers and friends, Dr. Weinan Leng, Dr. Harini Sooryanarain, Dr. AJ Prussin, Dr. Eric Vejerano, Dr. Andrea Tiwari, Dr. Mingjie Xie, Virginia Breazeal, Haoran Wei, Ray David, Peeyush Khare, Bardia Heidari Haratmeh. It's my honor to work with these talented and warm-hearted people.

At last, I want to express my gratitude to my parents, Degui Liu and Ruwen Zhou, who always selflessly support their son both materially and spiritually.

ATTRIBUTION

My advisor provided lots of beneficial suggestions to polish my writing. Several colleagues and professors aided in the design of experiments and manuscript drafting for one chapter of my thesis.

Chapter 2: One-Step Centrifugal Isolation of PEGylated Gold Nanoclusters for Single-Nanocluster Surface-Enhanced Raman Scattering

Chapter 2 was submitted to SMALL.

Weinan Leng, Ph.D (Laboratory for Environmental Nano-science and Technology, Department of Civil & Environmental Engineering) is a research scientist at Virginia Tech. Dr. Leng was a co-author on this paper and helped with the Raman imaging.

Linsey C. Marr, Ph.D (Laboratory for Environmental Nano-science and Technology, Department of Civil & Environmental Engineering) is a professor in the CEE department at Virginia Tech. Dr. Marr was a co-author on this paper, principal investigator for one of the grants that support the research, and contributed to the design of experiments and editorial comments.

Peter J. Vikesland, Ph.D (Laboratory for Environmental Nano-science and Technology, Department of Civil & Environmental Engineering) is a professor in the CEE department at Virginia Tech. Dr. Vikesland was the corresponding author on this paper, co-principal investigator for one of the grants that support the research, and contributed to the design of experiments and editorial comments.

Table of Contents

List of Figures

List of Tables

Chapter 1. Introduction and Literature Review

1.1 Introduction

Gold nanoparticles (AuNPs) are widely used in biological and chemical detection[1-3] due to their unique optoelectronic properties[4-9] and ease of surface modification using appropriate ligands[10-12]. AuNP-based biosensors have been developed for the analysis of metal ions, anions, small organic molecules, oligonucleotides, proteins, and small microorganisms including viruses, bacteria, and cancer cells.[1,2] Surface-enhanced Raman scattering (SERS) at the interface of gold or silver nanostructure and surface-bound molecules has enabled one of the most sensitive detection methods available for single molecule analysis.[13,14] SERS tags, which are novel nano-probes that combine metallic nanoparticles, a Raman reporter, surface coating for protection, and a layer of targeting molecules, have attracted enormous interest in the application of SERS-based biosensors.[15]

This thesis research was motivated by the goal of developing a novel AuNP-based biosensor to detect influenza virus with the aid of an ultrasensitive SERS tag. Chapter 1 presents a brief literature review of SERS, including fabrication and application of SERS tags. Chapter 2 describes a method to prepare high-purity, dye-tagged, polyethylene glycol (PEG)-encapsulated gold nanoclusters for single-nanocluster SERS imaging. Chapter 3 reports two methods to functionalize gold nanoparticles with aptamers that specifically recognize influenza virus.

1.2 Surface-enhanced Raman scattering

Raman scattering is a kind of inelastic scattering of a photon from a molecule in which the frequency change precisely matches the difference in vibrational energy levels[16].

Direct application of Raman scattering for trace analyte detection is limited, since the Raman scattering cross sections for molecules are usually too small to be detected[2]. In 1974, Fleischmann et al.[17] observed intense Raman scattering from pyridine adsorbed onto a roughened silver electrode. The dramatic enhancement of the Raman signal when the molecules happen to be adsorbed by gold or silver nanostructures, which was later recognized as SERS, redefined Raman scattering as an ultrasensitive approach for trace analyte detection. In 1997, Nie[14] and Kneipp[13] independently demonstrated the capability for single molecule detection using silver nanoparticles as a SERS substrate. The great enhancement of SERS intensity is often attributed to an electromagnetic enhancement mechanism[18] and a chemical enhancement mechanism[19]. The electromagnetic mechanism emphasizes enhancement of the electromagnetic field on metal surfaces caused by the excitation of the local surface plasmon resonance (LSPR) with incident light[20]. The chemical mechanism focuses on changes in the electronic structure of adsorbed molecules, which lead to resonant Raman scattering[21].

1.3 Nanocluster-Based SERS Substrate

Although single silver or gold nanoparticles have been used for SERS detection[22], aggregates of gold or silver nanoparticles have attracted more interest as SERS substrates. It has been recognized that nanometer-scale junctions[23,24] within multicore nanoclusters enhance the Raman signal such that single molecule detection is feasible[13,14]. These nanosized gaps are often referred as "hot-spots"[25] for the reason that the distribution of the enhancement factor decreases away the center following a power law[26]. Since the Raman signal enhanced by clusters is much higher than that of monomers[25,27-29], there has been enormous effort to fabricate cluster-based SERS

substrates[30-32]. One of the shortcomings of these cluster-based substrates is the challenge of controlled aggregation[29]; while homogeneous and pure aggregates are desirable, they are difficult to generate or isolate. Post-fabrication separation is therefore necessary to remove inactive single-core monomers and obtain homogeneous clusters[28].

Past researchers have exploited density or viscosity gradient centrifugation for size and shape selection of nanostructures, including metal nanoparticles,[29,33-38] carbon nanotubes,[39] and graphene[40]. Chen et al.[34] used a CsCl gradient for high-purity separation of amphiphilic-diblock-copolymer-coated 15 nm gold nanoparticle dimers and trimers. Tyler et al.[29] reported the removal of SERS-inactive, silica-encapsulated, dye-tagged monomers from SERS-active multimers using a viscosity gradient of iodixanol. Steinigeweg et al.[35] separated silica-encapsulated gold nanoclusters in the 30-80 nm size range in a density gradient of glycerol/water solutions and tested the single-particle SERS sensitivity of 60 nm gold nanoparticle dimers.

In Chapter 2, we build upon these previous efforts and report an efficient, low-cost isolation method that employs one-step centrifugation to isolate PEG-coated, dye-labeled, gold nanoclusters from a heterogeneous population.

1.4 SERS Tags and the Modification of Biomolecules to Gold Nanoparticles

SERS tags are novel nano-probes that combine gold or silver nanoparticles, Raman reporters, surface coating for protection, and a layer of targeting molecules.[15] Raman reporters signal the sensing event while the targeting molecules specifically bind to the compound of interest. The fabrication of SERS tags requires proper modification of metallic nanoparticles with specific targeting molecules such as antibodies, aptamers, or small-molecule ligands. In the design of AuNP immunosensors, antibodies are coupled to

AuNP-based transducers. For example, Qian et al.[22] developed a SERS tag composed of PEGylated AuNP and ScFv antibodies and achieved *in vivo* targeting of tumors. The hybridization of complementary single-stranded oligonucleotides is often exploited in SERS detection of DNA or RNA targets. Cao et al.[41] labeled 13 nm AuNPs with Raman dye-labeled oligonucleotides for DNA and RNA detection.

Aptamers are oligonucleotides with high binding affinity to given ligands that originate from a process termed "systematic evolution of ligands by exponential enrichment" (SELEX)[42]. Aptamers have several advantages over antibodies, which include low-cost, ease of synthesis, long-term stability, low immunogenicity, and greater tissue penetration[43]. Aptamer-based sensors, or aptasensors, using AuNPs have been applied to detect small molecules[44,45], proteins[46,47], viruses[48] and bacteria[49]. For example, Chung et al.[50] accomplished trace analysis of mercury ions using SERS tags modified with aptamers recognizing mercury ions exclusively.

Various approaches have been utilized to functionalize gold nanoparticles with biomolecules. Due to the strong affinity between gold surface and sulfhydryl groups, biomolecules modified with sulfhydryl groups easily bind to gold nanoparticles. AuNP functionalization with oligonucleotides is often realized by capping AuNP with (alkanethiol)-oligonucleotides[51-53]. The self-assembly of proteins on AuNPs[54-56], due to electrostatic binding and Au-amino acid (lysine, histidine, cysteine) interaction[55], is a common way to modify AuNPs with antibodies[57-59]. Streptavidin or avidin can thus be conjugated to AuNPs and facilitate the functionalization with biotin-labeled molecules[60], due to the strong conjugation between streptavidin (avidin) and biotin.

Silica coating of the AuNPs enhances stability, reduces nonspecific binding, and facilitates further modification under physiological conditions[15]. Sendroiu et al.[61] developed a DNA biosensor via direct modification of silica-coated AuNPs with complementary DNA. Similar to silica coating, PEG coating is another mature encapsulation method to fabricate gold-biomolecule hybrids with low toxicity, weak affinity to interference molecules, and excellent *in vivo* bio-distribution[62-64]. For example, Qian et al.[22] modified AuNP with HS-PEG-COOH followed by antibody conjugation with the aid of coupling reagents N-(3-dimethylaminopropyl)-N'-ethylcarbodiimide hydrochloride (EDC) and N-hydroxysulfosuccinimide (sulfo-NHS).

In Chapter 3, we report two methods of AuNP functionalization with single-stranded DNA aptamers against swine influenza H3N2 viruses[65]. Both methods take advantage of the strong binding between streptavidin and biotin-labeled aptamers. The first method involves the PEGylation of AuNPs followed by streptavidin conjugation with the aid of coupling reagents EDC and sulfo-NHS. The second method utilizes the self-assembly of streptavidin on AuNPs.

1.5 References

(1) Jans, H.; Huo, Q. *Chemical Society Reviews* **2012**, *41*, 2849.

(2) Saha, K.; Agasti, S. S.; Kim, C.; Li, X.; Rotello, V. M. *Chemical Reviews* **2012**, *112*, 2739.

(3) Wilson, R. *Chemical Society Reviews* **2008**, *37*, 2028.

(4) Elghanian, R.; Storhoff, J. J.; Mucic, R. C.; Letsinger, R. L.; Mirkin, C. A. *Science* **1997**, *277*, 1078.

(5) Storhoff, J. J.; Lazarides, A. A.; Mucic, R. C.; Mirkin, C. A.; Letsinger, R. L.; Schatz, G. C. *Journal of the American Chemical Society* **2000**, *122*, 4640.

(6) Rechberger, W.; Hohenau, A.; Leitner, A.; Krenn, J. R.; Lamprecht, B.; Aussenegg, F. R. *Optics Communications* **2003**, *220*, 137.

(7) Daniel, M.-C.; Astruc, D. *Chemical Reviews* **2004**, *104*, 293.

(8) Kelly, K. L.; Coronado, E.; Zhao, L. L.; Schatz, G. C. *The Journal of Physical Chemistry B* **2003**, *107*, 668.

(9) Nehl, C. L.; Liao, H.; Hafner, J. H. *Nano Letters* **2006**, *6*, 683.

(10) Katz, E.; Willner, I. *Angewandte Chemie International Edition* **2004**, *43*, 6042.

(11) Mout, R.; Moyano, D. F.; Rana, S.; Rotello, V. M. *Chemical Society Reviews* **2012**, *41*, 2539.

(12) Sperling, R. A.; Parak, W. J. *Surface modification, functionalization and bioconjugation of colloidal inorganic nanoparticles*, 2010; Vol. 368.

(13) Kneipp, K.; Wang, Y.; Kneipp, H.; Perelman, L. T.; Itzkan, I.; Dasari, R. R.; Feld, M. S. *Physical Review Letters* **1997**, *78*, 1667.

(14) Nie, S.; Emory, S. R. *Science* **1997**, *275*, 1102.

(15) Wang, Y.; Yan, B.; Chen, L. *Chemical Reviews* **2013**, *113*, 1391.

(16) Stiles, P. L.; Dieringer, J. A.; Shah, N. C.; Van Duyne, R. P. *Annual Review of Analytical Chemistry* **2008**, *1*, 601.

(17) Fleischmann, M.; Hendra, P. J.; McQuillan, A. J. *Chemical Physics Letters* **1974**, *26*, 163.

(18) Xu, H.; Aizpurua, J.; Käll, M.; Apell, P. *Physical Review E* **2000**, *62*, 4318.

(19) Campion, A.; Ivanecky, J. E.; Child, C. M.; Foster, M. *Journal of the American Chemical Society* **1995**, *117*, 11807.

(20) Haynes, C. L.; McFarland, A. D.; Duyne, R. P. V. *Analytical Chemistry* **2005**, *77*, 338 A.

(21) Campion, A.; Kambhampati, P. *Chemical Society Reviews* **1998**, *27*, 241.

(22) Qian, X.; Peng, X.-H.; Ansari, D. O.; Yin-Goen, Q.; Chen, G. Z.; Shin, D. M.; Yang, L.; Young, A. N.; Wang, M. D.; Nie, S. *Nat Biotech* **2008**, *26*, 83.

(23) Camden, J. P.; Dieringer, J. A.; Wang, Y. M.; Masiello, D. J.; Marks, L. D.; Schatz, G. C.; Van Duyne, R. P. *J Am Chem Soc* **2008**, *130*, 12616.

(24) Michaels, A. M.; Jiang, J.; Brus, L. *J Phys Chem B* **2000**, *104*, 11965.

(25) Wustholz, K. L.; Henry, A.-I.; McMahon, J. M.; Freeman, R. G.; Valley, N.; Piotti, M. E.; Natan, M. J.; Schatz, G. C.; Duyne, R. P. V. *Journal of the American Chemical Society* **2010**, *132*, 10903.

(26) Le Ru, E.; Etchegoin, P.; Meyer, M. *The Journal of chemical physics* **2006**, *125*, 204701.

(27) Talley, C. E.; Jackson, J. B.; Oubre, C.; Grady, N. K.; Hollars, C. W.; Lane, S. M.; Huser, T. R.; Nordlander, P.; Halas, N. J. *Nano Letters* **2005**, *5*, 1569.

(28) Chen, G.; Wang, Y.; Yang, M.; Xu, J.; Goh, S. J.; Pan, M.; Chen, H. *Journal of the American Chemical Society* **2010**, *132*, 3644.

(29) Tyler, T. P.; Henry, A. I.; Van Duyne, R. P.; Hersam, M. C. *J Phys Chem Lett* **2011**, *2*, 218.

(30) Sun, L.; Sung, K. B.; Dentinger, C.; Lutz, B.; Nguyen, L.; Zhang, J. W.; Qin, H. Y.; Yamakawa, M.; Cao, M. Q.; Lu, Y.; Chmura, A. J.; Zhu, J.; Su, X.; Berlin, A. A.; Chan, S.; Knudsen, B. *Nano Lett* **2007**, *7*, 351.

(31) Brown, L. O.; Doorn, S. K. *Langmuir* **2008**, *24*, 2277.

(32) Schwartzberg, A. M.; Grant, C. D.; Wolcott, A.; Talley, C. E.; Huser, T. R.; Bogomolni, R.; Zhang, J. Z. *The Journal of Physical Chemistry B* **2004**, *108*, 19191.

(33) Sun, X. M.; Tabakman, S. M.; Seo, W. S.; Zhang, L.; Zhang, G. Y.; Sherlock, S.; Bai, L.; Dai, H. J. *Angew Chem Int Edit* **2009**, *48*, 939.

(34) Chen, G.; Wang, Y.; Tan, L. H.; Yang, M. X.; Tan, L. S.; Chen, Y.; Chen, H. Y. *J Am Chem Soc* **2009**, *131*, 4218.

(35) Steinigeweg, D.; Schutz, M.; Salehi, M.; Schlucker, S. *Small* **2011**, *7*, 2443.

(36) Tyler, T. P.; Lin, P. A.; Tian, Y.; Gao, H.-J.; Gao, X. P. A.; Sankaran, R. M.; Hersam, M. C. *The Journal of Physical Chemistry Letters* **2012**, *3*, 1484.

(37) Bai, L.; Ma, X.; Liu, J.; Sun, X.; Zhao, D.; Evans, D. G. *J Am Chem Soc* **2010**, *132*, 2333.

(38) Bonaccorso, F.; Zerbetto, M.; Ferrari, A. C.; Amendola, V. *The Journal of Physical Chemistry C* **2013**, *117*, 13217.

(39) Arnold, M. S.; Green, A. A.; Hulvat, J. F.; Stupp, S. I.; Hersam, M. C. *Nat Nanotechnol* **2006**, *1*, 60.

(40) Green, A. A.; Hersam, M. C. *Nano Lett* **2009**, *9*, 4031.

(41) Cao, Y. C.; Jin, R.; Mirkin, C. A. *Science* **2002**, *297*, 1536.

(42) Hermann, T.; Patel, D. J. *Science* **2000**, *287*, 820.

(43) Tan, W.; Donovan, M. J.; Jiang, J. *Chemical Reviews* **2013**, *113*, 2842.

(44) Kim, Y. S.; Kim, J. H.; Kim, I. A.; Lee, S. J.; Jurng, J.; Gu, M. B. *Biosensors and Bioelectronics* **2010**, *26*, 1644.

(45) Guo, S.; Du, Y.; Yang, X.; Dong, S.; Wang, E. *Analytical Chemistry* **2011**, *83*, 8035.

(46) Wei, H.; Li, B.; Li, J.; Wang, E.; Dong, S. *Chemical Communications* **2007**, 3735.

(47) Deng, C.; Chen, J.; Nie, Z.; Wang, M.; Chu, X.; Chen, X.; Xiao, X.; Lei, C.; Yao, S. *Analytical Chemistry* **2009**, *81*, 739.

(48) Torres-Chavolla, E.; Alocilja, E. C. *Biosensors and Bioelectronics* **2009**, *24*, 3175.

(49) Yuan, J.; Wu, S.; Duan, N.; Ma, X.; Xia, Y.; Chen, J.; Ding, Z.; Wang, Z. *Talanta* **2014**, *127*, 163.

(50) Chung, E.; Gao, R.; Ko, J.; Choi, N.; Lim, D. W.; Lee, E. K.; Chang, S.-I.; Choo, J. *Lab on a Chip* **2013**, *13*, 260.

(51) Storhoff, J. J.; Elghanian, R.; Mucic, R. C.; Mirkin, C. A.; Letsinger, R. L. *Journal of the American Chemical Society* **1998**, *120*, 1959.

(52) Li, Z.; Jin, R.; Mirkin, C. A.; Letsinger, R. L. *Nucleic Acids Research* **2002**, *30*, 1558.

(53) Storhoff, J. J.; Elghanian, R.; Mirkin, C. A.; Letsinger, R. L. *Langmuir* **2002**, *18*, 6666.

(54) Kaufman, E. D.; Belyea, J.; Johnson, M. C.; Nicholson, Z. M.; Ricks, J. L.; Shah, P. K.; Bayless, M.; Pettersson, T.; Feldotö, Z.; Blomberg, E.; Claesson, P.; Franzen, S. *Langmuir* **2007**, *23*, 6053.

(55) Brewer, S. H.; Glomm, W. R.; Johnson, M. C.; Knag, M. K.; Franzen, S. *Langmuir* **2005**, *21*, 9303.

(56) Dobrovolskaia, M. A.; Patri, A. K.; Zheng, J.; Clogston, J. D.; Ayub, N.; Aggarwal, P.; Neun, B. W.; Hall, J. B.; McNeil, S. E. *Nanomedicine: Nanotechnology, Biology and Medicine* **2009**, *5*, 106.

(57) Mani, V.; Chikkaveeraiah, B. V.; Patel, V.; Gutkind, J. S.; Rusling, J. F. *ACS Nano* **2009**, *3*, 585.

(58) Driskell, J. D.; Jones, C. A.; Tompkins, S. M.; Tripp, R. A. *Analyst* **2011**, *136*, 3083.

(59) Liu, X.; Dai, Q.; Austin, L.; Coutts, J.; Knowles, G.; Zou, J.; Chen, H.; Huo, Q. *Journal of the American Chemical Society* **2008**, *130*, 2780.

(60) Kerman, K.; Chikae, M.; Yamamura, S.; Tamiya, E. *Analytica Chimica Acta* **2007**, *588*, 26.

(61) Sendroiu, I. E.; Warner, M. E.; Corn, R. M. *Langmuir* **2009**, *25*, 11282.

(62) Ishii, T.; Otsuka, H.; Kataoka, K.; Nagasaki, Y. *Langmuir* **2004**, *20*, 561.

(63) Cheng, Y.; C. Samia, A.; Meyers, J. D.; Panagopoulos, I.; Fei, B.; Burda, C. *Journal of the American Chemical Society* **2008**, *130*, 10643.

(64) Eck, W.; Craig, G.; Sigdel, A.; Ritter, G.; Old, L. J.; Tang, L.; Brennan, M. F.; Allen, P. J.; Mason, M. D. *Acs Nano* **2008**, *2*, 2263.

(65) Wongphatcharachai, M.; Wang, P.; Enomoto, S.; Webby, R. J.; Gramer, M. R.; Amonsin, A.; Sreevatsan, S. *Journal of Clinical Microbiology* **2013**, *51*, 46.

Chapter 2

One-Step Centrifugal Isolation of PEGylated Gold Nanoclusters for Single-Nanocluster Surface-Enhanced Raman Scattering

Xinzhe Zhou, Weinan Leng, Linsey C. Marr, Peter J. Vikesland*

Institute of Critical Technology and Applied Science (ICTAS) and Department of Civil and Environmental Engineering, Virginia Tech, Blacksburg, Virginia 24061, United States

The authors declare no competing financial interests.

2.1 Abstract

We report a method to prepare high-purity, dye-tagged, PEG-encapsulated gold nanoclusters for single-nanocluster surface enhanced Raman spectroscopy (SERS) imaging. Using density gradient centrifugation, SERS inactive monomers are removed from a population containing aggregates of varying size. High-purity small aggregates (2-4 nanospheres) and large aggregates (>5 nanospheres) can be separated after 15 min of centrifugation at 2500 × g. The purified nanoclusters produce a strong Raman signal when exposed to 0.5 mW laser power for only 0.2 s, enabling rapid Raman imaging.

2.2 Introduction

Ever since the discovery of single-molecule and single-nanoparticle surface-enhanced Raman scattering (SERS) in 1997,[1,2] it has been recognized that nanometer-scale junctions[3,4] within multicore nanoclusters enhance the Raman signal such that single molecule (SM) detection is feasible.[1] Salt-induced random aggregation was originally used to obtain Raman active nanoclusters.[5] Recently, however, charge neutralization of metal nanoparticles via surface modification with dye[6] has been exploited as an alternative strategy to prepare nanocluster-based SERS substrates.[7-10] Because aggregation is difficult to control via both salt- and dye-induced aggregation, post-

fabrication separation is needed to remove inactive single-core monomers and obtain pure Raman-active nanoclusters.[11,12]

Past researchers have exploited density or viscosity gradient centrifugation for size and shape selection of nanostructures, including metal nanoparticles,[11-17] carbon nanotubes,[18] and graphene[19]. Chen et al.[14] used a CsCl gradient for high-purity separation of amphiphilic diblock copolymer coated 15 nm gold nanoparticle dimers and trimers. Tyler et al.[11] reported the removal of SERS inactive, silica-encapsulated, dye-tagged monomers from SERS active multimers using a viscosity gradient of iodixanol. Steinigeweg et al.[12] separated silica-encapsulated gold nanoclusters in the 30-80 nm size range in a density gradient of glycerol/water solutions and tested the single-particle SERS sensitivity of 60 nm gold nanoparticle dimers. Herein, we build upon these previous efforts and report an efficient, low-cost isolation method that employs one-step centrifugation to isolate polyethylene glycol coated (i.e., PEGylated), dye-labeled, gold nanoclusters from a heterogeneous population (Figure 2-1). We then demonstrate the sensitivity of the individual nanoclusters for SERS imaging.

PEGylated gold nanoparticles (AuNP) are ideal for developing optical nanoprobes for bioanalysis because they are non-toxic, exhibit weak affinity to biomolecules, and have excellent in vivo biodistribution and pharmacokinetic properties.[20] To the best of our knowledge, no prior study has been conducted to prepare high-purity, PEGylated, nanocluster-based SERS probes.

2.3 Materials and Methods

2.3.1 Reagents and Materials

Chloroauric acid ($HAuCl_4 \bullet 3H_2O$), sodium citrate dehydrate, ethanol (98%), glycerol (99.9%), and Tween 20 were purchased from Sigma-Aldrich (St. Louis, MO). Malachite green isothiocyanate (MGITC) was purchased from Invitrogen Corp. (Grand Island, NY). Silicon wafers were obtained from Fisher Scientific (Pittsburg, PA). All glassware was cleaned with aqua regia (HCl: HNO_3, 3:1) followed by thorough rinsing with nanopure water prior to use.

2.3.2 Synthesis of AuNPs

55 nm gold nanoparticles were prepared according to the classic seed-mediated growth method.[10,21,22] Briefly, 200 μL of 1 M NaOH was added to 100 mL of 1 mM chloroauric acid solution to adjust the pH to 6.2-6.5. The solution was heated to a boil with vigorous stirring and 10 mL of 38.8 mM sodium citrate was added. After 15 min of reaction, when the solution attained a wine red color indicating the formation of 14 nm gold seeds, the seed solution was allowed to cool down to room temperature while being stirred. For the seed-mediated growth step, 500 mL of 0.254 mM $HAuCl_4$ solution was brought to a boil while being stirred, and then 2.2 mL of sodium citrate and 3.8 mL of as-synthesized seed solution were added to the boiling $HAuCl_4$ solution. After 30 min of reaction, the solution color turned pink, indicating the formation of 55 nm gold nanoparticles. The AuNP particle size was measured to be 55.3 ± 2.2 nm based upon an FESEM image analyzed by ImageJ software.

2.3.3 Dye-induced Aggregation of AuNP

Aliquots of 25 μM MGITC solution were added stepwise (10 μL each time) to 20 mL of AuNP solution while being stirred. The UV-Vis spectrum of the mixture was recorded after 50, 100, 150, 200, and 250 μL of MGITC solution had been added. After this

period, 14 μL of 1 mM carboxylated thiol-polyethyleneglycol (HS-PEG-COOH, MW ~ 3.4 kDa) was added to the solution, and it was stirred continuously for 15 min. Finally, 140 μL of excess HS-PEG (1 mM, MW ~ 5 kDa) was added to block the AuNP surface. After 30 min, 10 mL of 0.01% Tween 20 was added and the solution was centrifuged at 5000 × g for 20 min. The pellet was washed with 0.01% Tween 20 solution three times and resuspended in 2 mL ethanol.

2.3.4 Density Gradient Centrifugation

The density gradient was prepared by mixing different volume ratios of glycerol and ethanol. To produce the density gradient, 1.0 mL of 40% glycerol/ethanol solution was loaded to the bottom of a 5 mL polypropylene tube; 0.5 mL of 35%, 30%, 25%, and 20% glycerol/ethanol solutions were added thereafter. Prior to centrifugation, 200 μL of as-synthesized AuNP aggregates was carefully loaded on top of the density gradient, and the mixture was centrifuged at 2500 × g for 15 min. The separated bands were extracted using a 100 μL pipette and transferred to a 96-well plate. The UV-Vis spectra of the separated bands were recorded with a Safire2 microplate reader (Tecan Group Ltd, Switzerland). The Raman spectra were obtained using a WITec alpha500R microscope (Ulm, Germany) with a 10× objective (NA=0.3). Laser power of 0.5 mW and an integration time of 0.2 s were used. A 10 μL aliquot of each extracted band was applied to a clean silicon wafer using a spin coater (Laurell WS-400B-6NPP/LITE, Laurell Technologies Corp., PA) for SEM imaging with a LEO 1550 field-emission scanning electron microscope (FESEM; LEO Electron Microscopy Inc., Thorwood, NY) operated at an accelerating voltage of 10 kV. The number of monomers and aggregates in each

separated band were counted manually. Specifically, 500 nanoparticles were counted for bands b1 and b2 while 200 nanoparticles were counted for band b3.

The sedimentation coefficients (*s*) of the monomers and nanoclusters were calculated using the following equation:

$$s = \frac{m}{P(6\pi\eta r)}$$

where *m* is the particle mass, η is the viscosity of the medium, *r* is the effective diameter of an equivalent sphere with the same volume, and *P* is a geometrical correction factor for prolate ellipsoids. *P* was calculated using Perrin's equation:[23]

$$P = \frac{(1-q^2)^{1/2}}{q^{2/3} ln \frac{1+(1-q^2)^{1/2}}{q}}$$

where *q* is the ratio of the long axis to the short axis. To simplify the calculation, a monomer was treated as a 55 nm sphere, a dimer was treated as an ellipsoid with a short axis of 55 nm and q=2. Nanoclusters larger than dimers (n >2) were treated as straight-line configuration (q=n, short axis equals to 55 nm) to reflect the most extreme case. The sedimentation coefficients normalized to that of monomer are calculated. Results are shown in Figure 2-S2.

2.3.5 Single-Nanoparticle SERS

An aliquot of 2 μL of 10-fold diluted solution of b1, b2, and the mixture of b2 and b3 was spin-coated on a clean silicon wafer. The Raman images of several 15 μm × 15 μm areas (30 spots per line) for each sample were acquired with a 100× objective using 0.5 mW laser power and 0.2 s integration time for each spectrum obtained. The highest CCD count for each bright spot in the Raman image was recorded as the Raman intensity for

that spot. An FESEM image of the same location was captured for comparison with the corresponding Raman image.

2.4 Results and Discussion

Herein, PEGylated AuNPs were synthesized according to a published protocol.[24] Each AuNP was modified with 2000-3000 molecules of malachite green isothiocyanate (MGITC), which acts as a surface-bound Raman dye and induces formation of AuNP multimers.[10] The color change from pink to deep purple as well as the increase in optical absorption around 770 nm indicate aggregation of the AuNPs (Figure 2-S1). To prevent further aggregation of AuNPs and the loss of MGITC due to hydrolysis,[7] the MGITC-functionalized AuNPs were protected with HS-PEG-COOH (MW=3.4 kDa) followed by addition of excess HS-PEG (MW=5 kDa) to block the AuNP surface.

The PEGylated AuNPs were re-suspended in ethanol and loaded on top of a density gradient consisting of 20, 25, 30, 35, and 40% glycerol/ethanol solutions (Figure 2-1). After centrifugation at 2500 × g for 15 min using a desktop centrifuge (Jouan C3i, Thermo Electron Corp.), three distinct bands were separated and extracted. The size distributions of the as-synthesized product and separated bands were determined by manually counting several hundred nanoclusters in scanning electron microscopy (SEM) micrographs. The as-synthesized product typically contained 59% monomers, 13% dimers, 18% trimers, 7% tetramers, and 3% higher-order nanoclusters. The b1 band was composed primarily of monomers (98%) with a small amount of dimers (1%) and trimers (1%). The b2 band primarily contained small nanoclusters: 32% dimers, 45% trimers, 18% tetramers, and 5% higher-order aggregates. The remaining 0.5% of clusters were monomers. The b3 band was composed of 7.5% pentamers and 92% hexamers and

higher-order aggregates. The remaining 1% of clusters were tetramers and lower-order aggregates.

Sedimentation coefficients (*s*) were calculated for monomer, dimer, and larger nanoclusters (assumed to be in a linear configuration; Figure 2-S2). The *s* for a dimer is 52% percent larger than that of monomer. The slope of *s* versus the number of AuNPs in a nanocluster, *n*, decreases with increasing *n*. Trimers settle 22% faster than do dimers, while tetramers settle only 15% faster than trimers (Figure 2-S2). These results explain the good separation of monomers from the nanoclusters and the poorer separation of dimers, trimers, and tetramers from each other. Similar results were found in Tyler's[11] study of silica-encapsulated AuNP separation.

The red color (Figure 2-1B, 2-S1) and UV-Vis spectrum of b1 (Figure 2-1C, 2-S1) with peak absorbance at 531 nm were the same as for the AuNP stock suspension. This wavelength corresponds to a particle size of 50 nm,[25] a value which is similar to the SEM-based measurement of 55.3 ± 2.2 nm. In addition to the localized surface plasmon resonance band ($LSPR_1$) at 531 nm, a second band ($LSPR_2$) at 738 nm is apparent in the spectra of b2 and b3 (Figure 2-1C). The presence of $LSPR_2$ in b2 and b3 is indicative of multimers, while its absence from the b1 spectra indicates their absence. Furthermore, enhanced absorbance of b3 at λ>738 nm indicates the presence of very large aggregates. Addition of increasing amounts of MGITC promoted aggregation, as absorbance at 531 nm decreased while that at 738 nm increased (Figure 2-S1), thus confirming the distinction in optical properties between monomers and multimers.

The Raman intensity of the separated bands was measured at an excitation wavelength of 633 nm using a WITec Alpha 500R at a laser power of 0.5 mW for 0.2 s. The Raman

spectra exhibit characteristic bands for MGITC at 1171, 1364, and 1614 cm^{-1} that we assign to the in-plane benzene υ_9 mode, phenyl-N stretch, and phenyl-N + C-C stretch modes, respectively.[26-28] These bands shift slightly to 1176, 1367, and 1603 cm^{-1} for b2 and b3 (Figure 2-1D), while b1 exhibited none of these bands. This observation is consistent with the fact that b1 contained only a minimal number of residual multimers, while b2 and b3 were composed primarily of nanoclusters.

To identify the single-nanocluster SERS sensitivity of our multimers, 2 μL of 10× diluted b1 and b2 was spin-coated on a silicon chip and imaged sequentially by a field-emission scanning electron microscope (FESEM) and the Raman microscope. Comparison of the Raman image with an SEM image of the same location enabled investigation of the Raman intensity of individual nanoclusters. In agreement with the ensemble average Raman spectrum of b1, the Raman response of every monomer probed was too weak to be detected by our system. One dimer, two trimers, and one tetramer from b2 were examined in detail. All four multimers produced peaks indicative of MGITC at the same wavenumbers as the ensemble average spectrum of the b2 and b3 suspensions (Figure 2-1D, 2-2). However, there was no clear correlation between the aggregation state and the Raman intensity. The measured Raman intensity is known to be affected by shape, geometry,[3] orientation,[29,30] gap size,[31] and laser polarization.[32] For example, trimer a2 (V shape) and trimer a3 (triangle shape) differed in geometry and orientation, with trimer a2 (66 cts) exhibiting nearly twice the Raman intensity compared to trimer a3 (34 cts).

Taking advantage of the strong Raman intensity of the isolated nanoclusters, single-nanocluster SERS could be a powerful tool for ultrasensitive bio-imaging.[20] By binding

bio-functional ligands such as antibodies[24] or DNA[33] to the active carboxylated PEG of these isolated nanoclusters, Raman tags that specifically bind to biological targets can be developed. For example, Nie et. al.[24] successfully applied MGITC-tagged, PEGylated AuNP for in vivo tumor targeting. High-purity nanocluster-based Raman tags have the potential to significantly improve the sensitivity of pathogen detection, tumor imaging, tissue imaging, and other applications.[20] The high SERS sensitivity of these nanoclusters leads to a significant decrease in the required laser energy and integration time, thus enabling rapid, safe, and real-time SERS imaging.

A mixture of b2 and b3 was used to demonstrate the potential of nanoclusters for bio-imaging. In a SERS image of a 15 μm × 15 μm area (Figure 2-3A), four bright spots e, f, g, and h appear at the same locations as four corresponding nanoclusters including two octamers (E and F) and two trimers (G and H) found under FESEM (Figure 2-3B). Due to the diffraction of light, the theoretical optical resolution is limited to 0.61λ divided by the numerical aperture (N.A.)[34,35] or 430 nm using a 633 nm laser (N.A. = 0.9). However, the size of bright spots in our Raman image is much larger than 430 nm and in the range of 1-2 μm. For instance, the bright spot of octamer E covers at least 3 × 3 pixels (1.5 μm × 1.5 μm, Figure 2-4). The Raman intensity in the centroid is much higher than that of the edge, which is in accordance with the point spread function.[34,36] The distance between the centroid of each bright spot and nanocluster was measured. The lengths of ef, fg, gh, and eh were identical to those of EF, FG, GH, and EH, so it is highly likely that the signals from the bright spots originated from the four nanoclusters. The Raman intensities of the four nanoclusters fulfilled the requirement of high signal-to-noise ratio, ensuring sensitivity and accuracy of SERS imaging in this application (Figure 2-S3).

2.5 Conclusion

The novelty of this effort lies in the simplicity of the methods employed to reproducibly isolate dimers and trimers using readily available materials. The centrifuge used for these experiments was a simple bench-top model commonly available in many analytical chemistry and cell biology laboratories. Furthermore, the density gradient was prepared using glycerol and ethanol – two materials that are readily available and of substantially lower cost than iodixanol. As we have shown, AuNP-MGITC nanoclusters of distinct sizes can be isolated from a population of heterogeneous aggregates. Three distinct bands including monomers, small aggregates (2-4 nanospheres), and large aggregates (>5 nanospheres) can be separated via density gradient centrifugation. A new peak in optical absorbance at 738 nm is observed for the two isolated nanocluster suspensions. Under our imaging conditions (which are similar to those used in many non-Raman specialist laboratories) there was no reproducible correlation between the number of nanoparticles in a nanocluster and the Raman intensity and thus our method, which facilitates removal of non-active monomers, leads to more efficient single-nanocluster SERS imaging. High-purity nanoclusters are very promising in developing ultrasensitive Raman tags for SERS-based bio-imaging and biosensor applications.

2.6 Acknowledgments

This material is based upon work supported by the National Science Foundation through the Center for the Environmental Implications of Nanotechnology (DBI-1266252), the Virginia Tech Institute for Critical Technology and Applied Science (ICTAS), and the Virginia Tech Sustainable Nanotechnology (VTSuN) Interdisciplinary Graduate Education Program.

2.7 References

(1) Nie, S. M.; Emery, S. R. *Science* **1997**, *275*, 1102.

(2) Kneipp, K.; Wang, Y.; Kneipp, H.; Perelman, L. T.; Itzkan, I.; Dasari, R.; Feld, M. S. *Phys Rev Lett* **1997**, *78*, 1667.

(3) Camden, J. P.; Dieringer, J. A.; Wang, Y. M.; Masiello, D. J.; Marks, L. D.; Schatz, G. C.; Van Duyne, R. P. *J Am Chem Soc* **2008**, *130*, 12616.

(4) Michaels, A. M.; Jiang, J.; Brus, L. *J Phys Chem B* **2000**, *104*, 11965.

(5) Michaels, A. M.; Nirmal, M.; Brus, L. E. *J Am Chem Soc* **1999**, *121*, 9932.

(6) Faulds, K.; Littleford, R. E.; Graham, D.; Dent, G.; Smith, W. E. *Anal Chem* **2004**, *76*, 592.

(7) Brown, L. O.; Doorn, S. K. *Langmuir* **2008**, *24*, 2178.

(8) Brown, L. O.; Doorn, S. K. *Langmuir* **2008**, *24*, 2277.

(9) Sun, L.; Sung, K. B.; Dentinger, C.; Lutz, B.; Nguyen, L.; Zhang, J. W.; Qin, H. Y.; Yamakawa, M.; Cao, M. Q.; Lu, Y.; Chmura, A. J.; Zhu, J.; Su, X.; Berlin, A. A.; Chan, S.; Knudsen, B. *Nano Lett* **2007**, *7*, 351.

(10) Leng, W.; Vikesland, P. J. *Langmuir* **2014**, *30*, 8342.

(11) Tyler, T. P.; Henry, A. I.; Van Duyne, R. P.; Hersam, M. C. *J Phys Chem Lett* **2011**, *2*, 218.

(12) Steinigeweg, D.; Schutz, M.; Salehi, M.; Schlucker, S. *Small* **2011**, *7*, 2443.

(13) Sun, X. M.; Tabakman, S. M.; Seo, W. S.; Zhang, L.; Zhang, G. Y.; Sherlock, S.; Bai, L.; Dai, H. J. *Angew Chem Int Edit* **2009**, *48*, 939.

(14) Chen, G.; Wang, Y.; Tan, L. H.; Yang, M. X.; Tan, L. S.; Chen, Y.; Chen, H. Y. *J Am Chem Soc* **2009**, *131*, 4218.

(15) Tyler, T. P.; Lin, P. A.; Tian, Y.; Gao, H.-J.; Gao, X. P. A.; Sankaran, R. M.; Hersam, M. C. *The Journal of Physical Chemistry Letters* **2012**, *3*, 1484.

(16) Bai, L.; Ma, X.; Liu, J.; Sun, X.; Zhao, D.; Evans, D. G. *J Am Chem Soc* **2010**, *132*, 2333.

(17) Bonaccorso, F.; Zerbetto, M.; Ferrari, A. C.; Amendola, V. *The Journal of Physical Chemistry C* **2013**, *117*, 13217.

(18) Arnold, M. S.; Green, A. A.; Hulvat, J. F.; Stupp, S. I.; Hersam, M. C. *Nat Nanotechnol* **2006**, *1*, 60.

(19) Green, A. A.; Hersam, M. C. *Nano Lett* **2009**, *9*, 4031.

(20) Wang, Y. Q.; Yan, B.; Chen, L. X. *Chem Rev* **2013**, *113*, 1391.

(21) Brown, K. R.; Walter, D. G.; Natan, M. J. *Chem Mater* **2000**, *12*, 306.

(22) Frens, G. *Nature* **1973**, *241*, 20.

(23) Biddle, D.; Walldal, C.; Wall, S. *Colloid Surface A* **1996**, *118*, 89.

(24) Qian, X. M.; Peng, X. H.; Ansari, D. O.; Yin-Goen, Q.; Chen, G. Z.; Shin, D. M.; Yang, L.; Young, A. N.; Wang, M. D.; Nie, S. M. *Nat Biotechnol* **2008**, *26*, 83.

(25) Haiss, W.; Thanh, N. T. K.; Aveyard, J.; Fernig, D. G. *Anal Chem* **2007**, *79*, 4215.

(26) Li, M.; Zhang, J.; Suri, S.; Sooter, L. J.; Ma, D.; Wu, N. *Anal Chem* **2012**, *84*, 2837.

(27) Kaminska, A.; Dziecielewski, I.; Weyher, J. L.; Waluk, J.; Gawinkowski, S.; Sashuk, V.; Fialkowski, M.; Sawicka, M.; Suski, T.; Porowski, S.; Holyst, R. *Journal of Materials Chemistry* **2011**, *21*, 8662.

(28) Lueck, H. B.; Daniel, D. C.; McHale, J. L. *Journal of Raman Spectroscopy* **1993**, *24*, 363.

(29) Shegai, T.; Brian, B.; Miljkovic, V. D.; Kall, M. *Acs Nano* **2011**, *5*, 2036.

(30) Stranahan, S. M.; Titus, E. J.; Willets, K. A. *J Phys Chem Lett* **2011**, *2*, 2711.

(31) GarciaVidal, F. J.; Pendry, J. B. *Phys Rev Lett* **1996**, *77*, 1163.

(32) Steinigeweg, D.; Schutz, M.; Schlucker, S. *Nanoscale* **2013**, *5*, 110.

(33) Medley, C. D.; Bamrungsap, S.; Tan, W. H.; Smith, J. E. *Anal Chem* **2011**, *83*, 727.

(34) Stranahan, S. M.; Willets, K. A. *Nano Letters* **2010**, *10*, 3777.

(35) McLintock, A.; Cunha-Matos, C. A.; Zagnoni, M.; Millington, O. R.; Wark, A. W. *ACS Nano* **2014**, *8*, 8600.

(36) Titus, E. J.; Willets, K. A. *ACS Nano* **2013**, *7*, 6258.

2.8 Figures

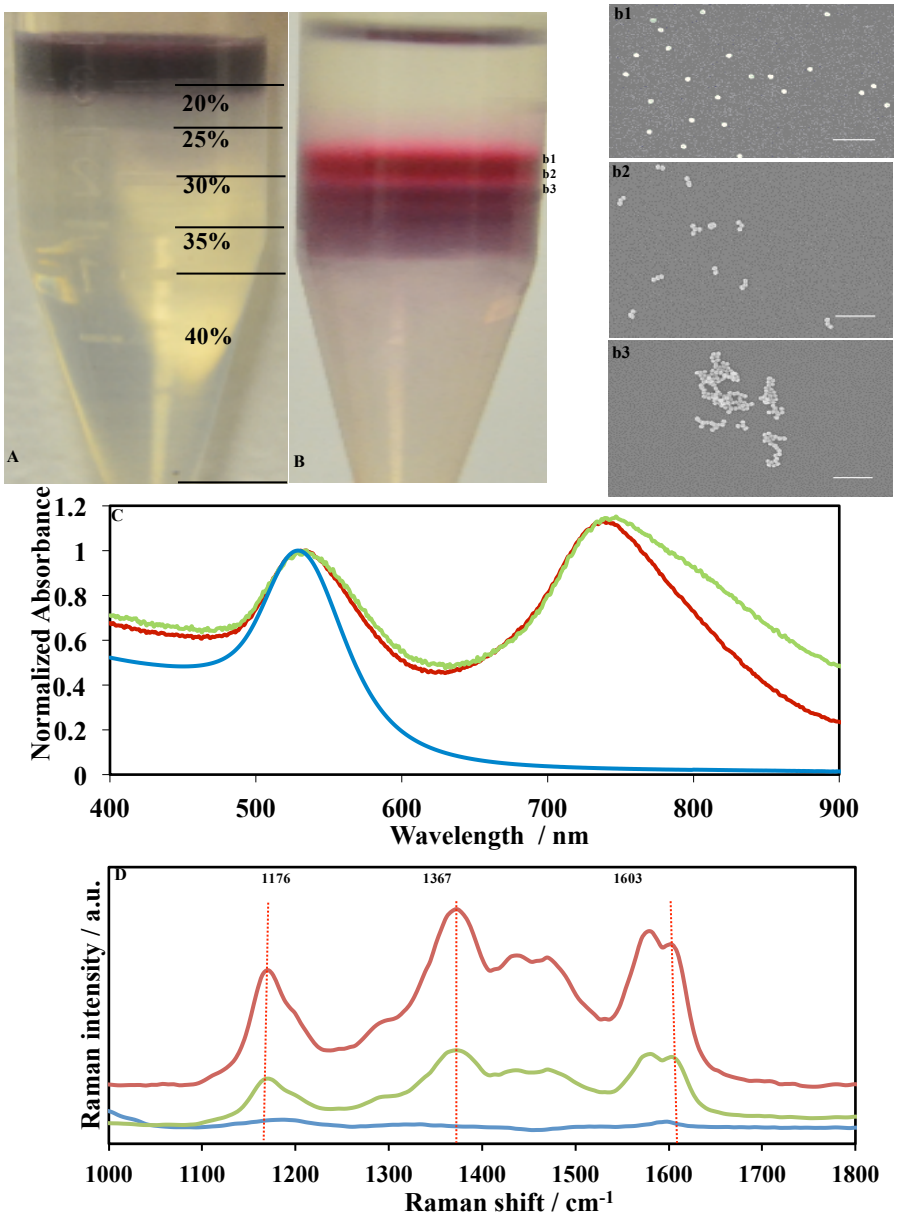

Figure 2-1. (A) An aliquot (0.2 mL) of concentrated, as-synthesized AuNPs loaded on top of a density gradient of 20, 25, 30, 35, and 40% glycerol/ethanol. (B) Three distinct bands (b1, b2, and b3) after density gradient centrifugation at 2500 × g for 15 min. FESEM images of nanoclusters within each band. Scale bar denotes 300 nm. (C) Normalized UV-Vis spectra of b1 (blue), b2 (red), and b3 (green) suspensions. (D) Raman spectra of b1, b2, and b3 suspensions.

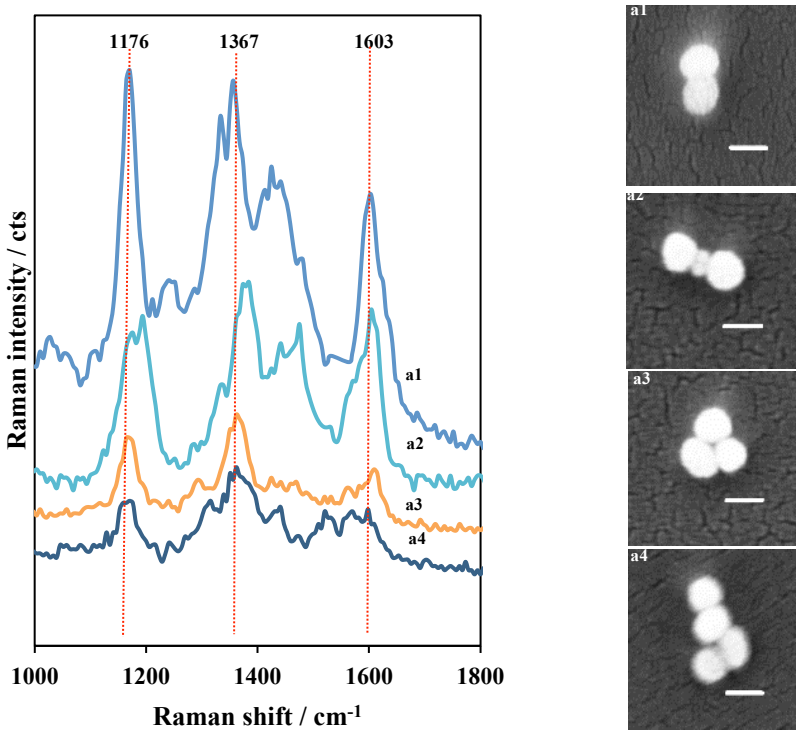

Figure 2-2. Raman spectra of four nanoclusters (a1, a2, a3, and a4) from the b2 band. FESEM images of the four nanoclusters. Scale bar denotes 50 nm.

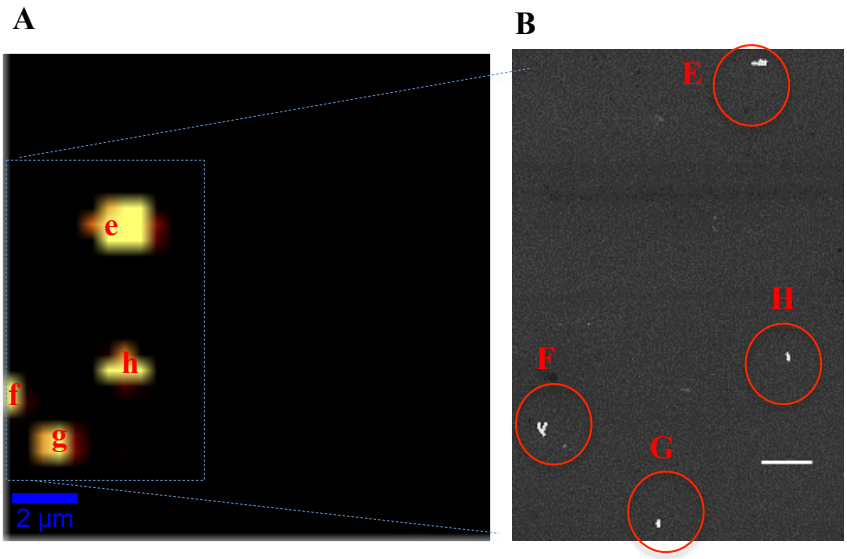

Figure 2-3. (A) Raman image scan of four nanoclusters from the mixture of b2 and b3 bands. (B) FESEM image of the same area as the dashed box in A. Scale bar denotes 1 µm.

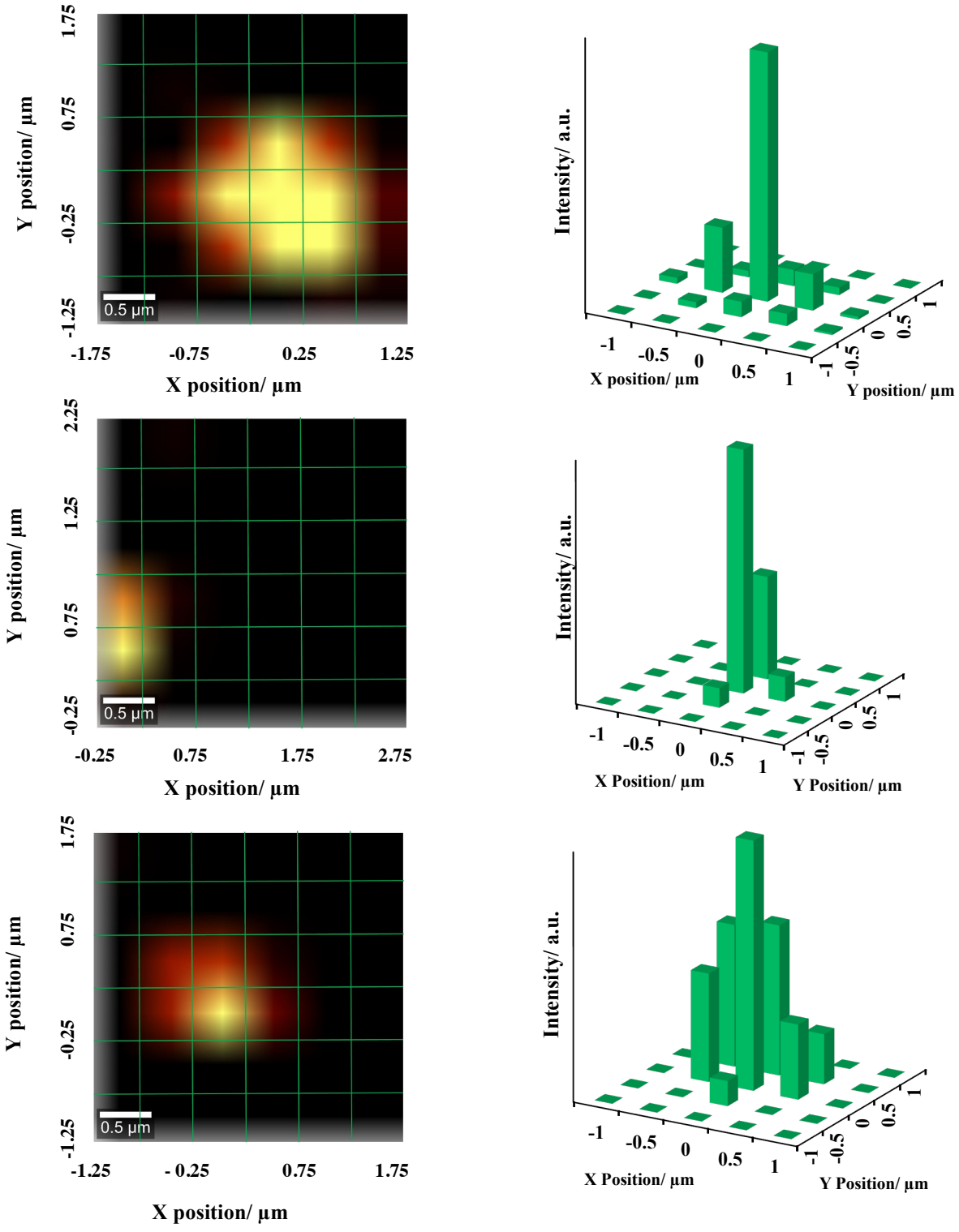
Y position/ µm
1.75
0.75
-0.25
-1.25
0.5 µm
-1.75
-0.75
0.25
1.25
X position/ µm
Intensity/ a.u.
-1
-0.5
0
0.5
1
X position/ µm
Y position/ µm
Y position/ µm
2.25
1.25
0.75
-0.25
0.5 µm
-0.25
0.75
1.75
2.75
X position/ µm
Intensity/ a.u.
X Position/ µm
Y Position/ µm
Y position/ µm
1.75
0.75
-0.25
-1.25
0.5 µm
-1.25
- 0.25
0.75
1.75
X position/ µm
Intensity/ a.u.
X Position/ µm
Y Position/ µm

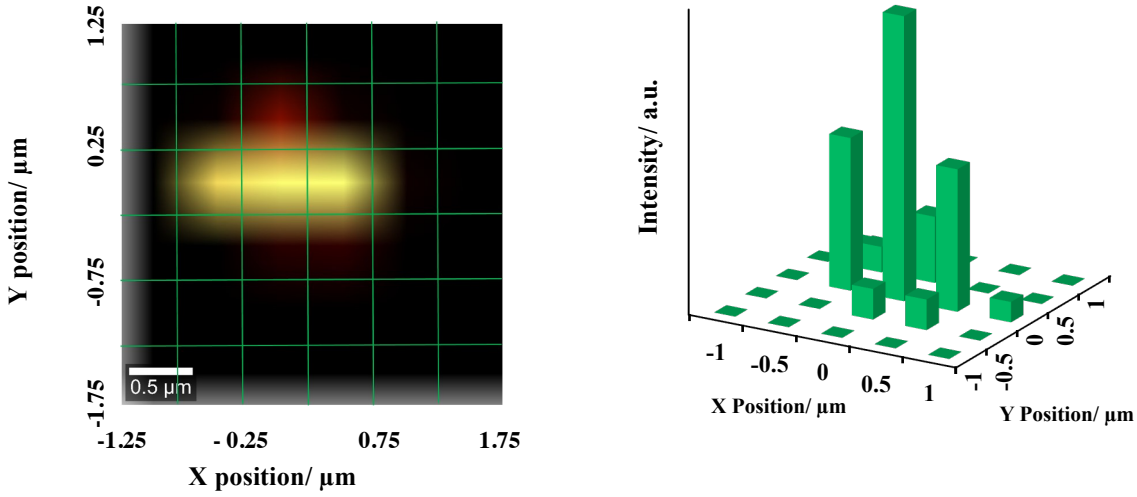

Figure 2-4. Top: Raman images of, top to bottom, nanoclusters E (octamer), F (octamer), G (trimer), and H (trimer) from Figure 2-3. Each square represents a 0.5 µm × 0.5 µm pixel. Bottom: Distribution of Raman intensity at 1603 cm^{-1} in the Raman image. The Raman intensity is normalized by the value at the centroid. Axes are shifted compared to the image above it so that the peak intensity appears in the center.

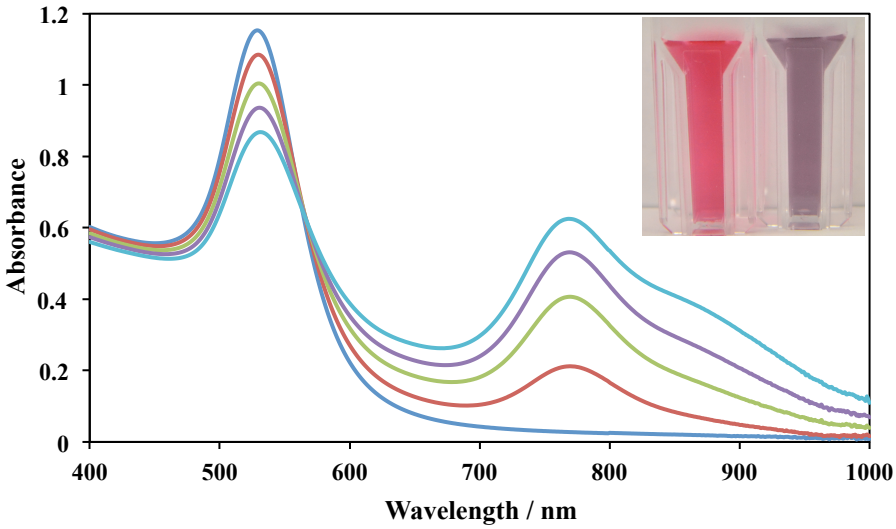

Figure 2-S1. UV-Vis spectra of AuNP suspensions as a function of the amount of MGITC applied. From top to bottom at 531 nm, each spectrum represents an MGITC/AuNP ratio of 500, 1000, 1500, or 2000. Inset: color change before (left) and after (right) MGITC addition.

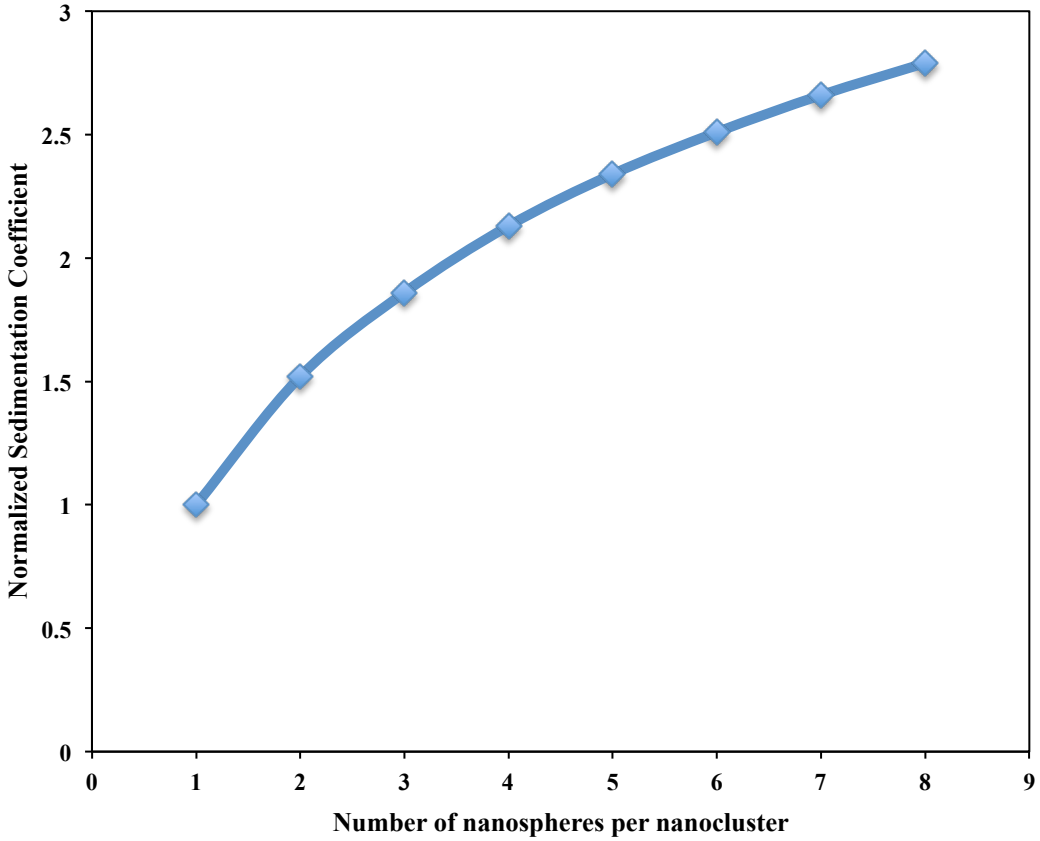

Figure 2-S2. Normalized sedimentation coefficients of nanoclusters assuming a straight-line configuration for nanoclusters with the number of nanospheres per cluster ($\geq$ 2).

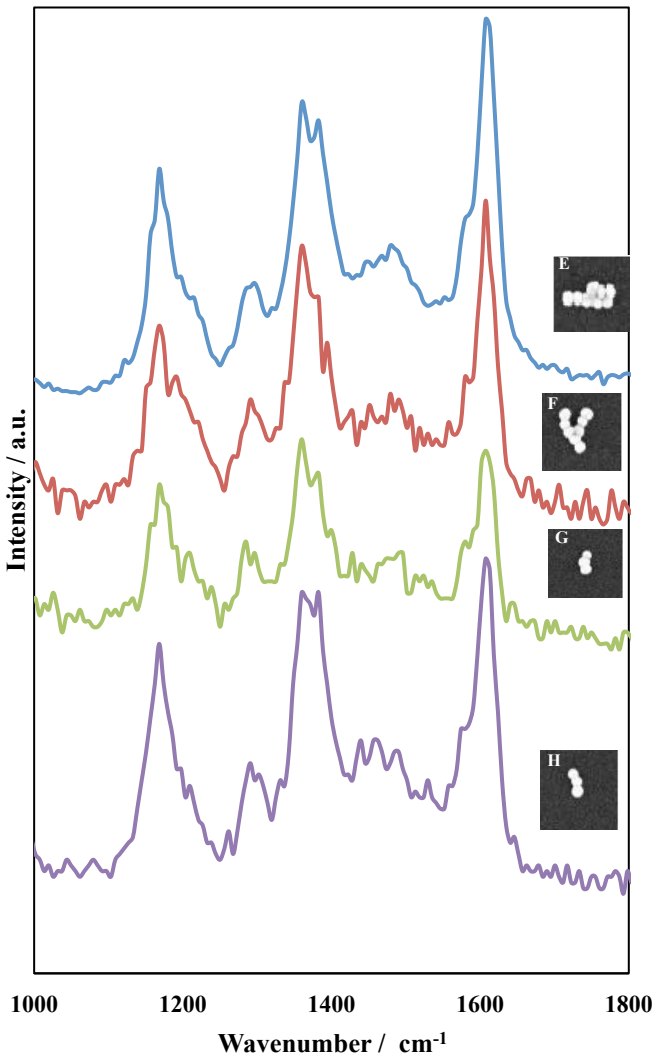

Figure 2-S3. SERS spectra of the four bright spots in Figure 2B. The Raman intensity of E is divided by 10 to enable it to fit on the same scale. Inset: FESEM images of the four nanoclusters in Figure 2-3B.

Chapter 3

Functionalization of Gold Nanoparticles with Aptamers

3.1 Introduction

Gold nanoparticles (AuNPs) are widely used in biological and chemical detection and sensing[1-3] due to their unique optical properties[4-9] and ease of surface modification using appropriate ligands[10-12]. Colorimetric sensing based on inter-particle surface plasmon coupling is a very popular strategy for any target analyte that triggers the aggregation or re-dispersion of AuNPs.[4,13-15] Surface-enhanced Raman scattering (SERS) at the interface of AuNPs and surface-bound molecules is one of the most sensitive detection schemes for single molecule analysis.[16,17] AuNP-based biosensors have been developed for the analysis of metal ions, anions, small organic molecules, oligonucleotides, proteins, and small microorganisms including viruses, bacteria, and cancer cells.[1,2]

One major category of sensing platform employs labeling, or attaching specific recognition moieties to the AuNP core. For example, SERS tags are novel nano-probes that combine metallic nanoparticles, a Raman reporter, surface coating for protection, and a layer of targeting molecules.[18] In the design of AuNP immunosensors, antibodies are coupled to AuNP-based transducers. For example, Qian et al.[19] developed a SERS tag composed of PEGylated AuNP and ScFv antibodies and achieved *in vivo* tumor targeting. Driskell et al.[20] detected influenza virus with AuNPs conjugated with antibodies specific to H1N1 influenza virus. Complementary oligonucleotides are often used to recognize DNA target in colorimetric biosensors[4,14,21]. Li et al. developed a colorimetric detection platform for DNA sequences based on electrostatic interaction with unmodified gold nanoparticles[14].

Aptamers are oligonucleotides with high binding affinity to given ligands that originate from a process termed "systematic evolution of ligands by exponential enrichment" (SELEX)[22]. Aptamers have several advantages over antibodies, which include low cost, ease of synthesis, long-term stability, low immunogenicity, and greater tissue penetration[23]. Aptamer-based sensors, or aptasensors, using AuNPs have been applied to detect small molecules[24,25], proteins[26,27], viruses[28] and bacteria[29].

Herein, we report two methods of AuNP functionalization with single-stranded DNA aptamers against swine influenza H3N2 viruses[30]. Both methods take advantage of the strong binding between streptavidin and biotin-labeled aptamers. The first method involves the coating of AuNPs with polyethylene glycol (PEG) followed by streptavidin conjugation with the aid of coupling reagents. The second method utilizes the self-assembly of streptavidin on AuNPs. The structures of aptamer-modified AuNPs fabricated via these two methods are shown in Figure 3-1.

3.2 Materials and Methods

3.2.1 Reagents and Materials

Chloroauric acid ($HAuCl_4 \bullet 3H_2O$), sodium citrate dehydrate, N-(3-dimethylaminopropyl)-N'-ethylcarbodiimide hydrochlorideand (EDC), N-hydroxysulfosuccinimide (sulfo-NHS), streptavidin (SA), bovine serum albumin (BSA), and Tween 20 were purchased from Sigma-Aldrich (St. Louis, MO). A 5'-biotin-aptamer with sequence specific to H3N2, TTTTTTTTTTGTGCAGTCAAAGACGTCCACTCCGTCATCTTTAGTGGCCCCAATGTCGTTATCACCGAGACCATGAAGTGCGATTGCC[30], was purchased from Invitrogen. All reagents were used as received without further treatment. All glassware

was cleaned with aqua regia ($HCl:HNO_3$, 3:1) followed by thorough rinsing with deionized water prior to use.

3.2.2 Synthesis of AuNPs

50 nm gold nanoparticles were prepared according to the classic seed-mediated growth method.[31-33] Briefly, 200 μL of 1 M NaOH was added to 100 mL of 1 mM chloroauric acid solution to adjust the pH to 6.2-6.5. The solution was heated to a boil with vigorous stirring, and 10 mL of 38.8 mM sodium citrate was added. After 15 min of reaction, when the solution attained a wine red color indicating the formation of 14 nm gold seeds, the seed solution was allowed to cool down to room temperature while being stirred. For the seed-mediated growth step, 500 mL of 0.254 mM $HAuCl_4$ solution was brought to a boil while being stirred, and then 2.2 mL of sodium citrate and 3.8 mL of as-synthesized seed solution were added to the boiling $HAuCl_4$ solution. After 30 min of reaction, the solution color turned pink, indicating the formation of 50 nm gold nanoparticles.

3.2.3 AuNP functionalization via PEGylation

100 μL of 10 μM carboxylated thiol-polyethyleneglycol (HS-PEG-COOH, MW ~ 3.5 kDa) was added to 1.7 mL of AuNP solution, and it was stirred continuously for 30 min. Thereafter, 100 μL of excess HS-PEG (100 μM, MW ~5 kDa) was added to block the AuNP surface. After 30 min, 10 μL of 1% Tween 20 was added, and the solution was centrifuged at 3000 × g for 15 min. The pellet was washed with 1 mL of 0.01% Tween 20 three times and re-suspended in 1 mL of MES buffer (10 mM, pH=5.5).

1 mg of EDC and 2 mg of sulfo-NHS powder were dissolved with the washed PEGylated AuNP solution to activate the –COOH groups and convert it into a semi-stable sulfo-NHS ester. After 15 min of incubation, the solution was centrifuged at 3000

× g for 15 min. The pellet was re-suspended in 1 mL of streptavidin solution (0.1 mg/mL, 10 mM HEPES buffer) to complete the conjugation between the NHS-esters and streptavidin (-NH_2 group). The solution was then incubated for 2 hours.

Excess streptavidin was removed via three rounds of centrifugation (3000 × g for 15 min) and re-suspension in 10 mM HEPES buffer. 100 μL of 5'-biotin-aptamer (100 μM) was added to the AuNP-PEG-streptavidin solution. The mixture was incubated overnight and then washed with 10 mM PBS buffer four times. The final product was re-suspended in 1 mL of 10 mM PBS buffer and stored at 4 °C.

3.2.4 AuNP functionalization via Adsorption

Prior to functionalization, the AuNP solution was adjusted to a pH of 7.2 with 0.1 M K_2CO_3. 100 μL of 1 mg/ml streptavidin was added to 1 mL of AuNP solution. After 30 min of incubation, 10% BSA was added to block the AuNP surface. The solution was centrifuged at 3000 × g for 15 min. The pellet was washed with 1 mL of 1% BSA three times and re-suspended in 1mL of 1% BSA (10 mM DPBS buffer, pH=7.4). 100 μL of 5'-biotin-aptamer was added to the AuNP-streptavidin solution. The mixture was incubated overnight and then washed with 1% BSA four times. The final product was re-suspended in 1 mL of 10 mM DPBS buffer and stored at 4 °C.

3.2.5 Characterization with DLS and UV-vis Spectrometer

The particle size of intermediate and final products was measured using a Zetasizer NanoZS instrument (Malvern Instruments, UK) with a 173° scattering angle at room temperature. The optical absorbance spectra were acquired with a Cary 5000 double-beam UV−vis−NIR spectrophotometer.

3.3 Results and Discussion

3.3.1 AuNP Functionalization via PEGylation

The PEG coating induced a 2 nm redshift of the localized surface plasmon resonance (LSPR) band of AuNP (Figure 3-2A), indicating a change in the local dielectric environment[34]. Due to the formation of a thick layer of PEG, further modification with streptavidin and aptamer did not affect the LSPR band of PEGylated AuNP (Figure 3-2A). The hydrodynamic diameter (HD) increased by 21.9 nm after PEGylation as measured by DLS (Figure 3-2B). The conjugation of amine groups presented on streptavidin and the activated semi-stable sulfo-NHS ester resulted in a 2.7 nm size change of the PEGylated AuNP. As X-ray analysis[35] reveals streptavidin to be 5 nm in size, an increase of 10 nm was expected if a streptavidin monolayer formed on the AuNP surface. Therefore, the PEGylated AuNP was not fully covered by streptavidin after the conjugation. The intermediate product AuNP-PEG-SA was then reacted readily with 5'-biotin-aptamer via the streptavidin-biotin reaction. An 11.2 nm increase in HD was observed.

3.3.2 AuNP functionalization via adsorption

After the adsorption of SA and BSA to AuNP, the HD of AuNP increased by 16.5 nm (Figure 3-3B), and the LSPR band red-shifted by 5 nm (Figure 3-3A). Brewer et al.[36] suggested two mechanisms for the interaction between BSA and citrate-coated AuNP. The first is electrostatic binding, which emphasizes the attraction between the positive surface residues (i.e., lysine) of BSA and the negative charge from the citrate. The second is displacement, requiring the displacement of citrate by BSA with the amino acids lysine (amine), histidine (imidazole), and cysteine (thiol) that directly interact with the gold

surface. Via displacement of citrate by SA and BSA, the change in the local dielectric environment[34] of AuNP has been shown to contribute to the 5 nm shift of the LSPR band. A similar LSPR shift was also reported for a AuNP-HSA (human serum albumin) bio-conjugate by Cañaveras et al.[37]. Similar to PEG coating, the protein coating on AuNPs inhibited further shifts in the UV-vis spectrum of AuNP-SA-biotin-aptamer compared to that of AuNP-SA (Figure 3-3A), indicating no change of the local dielectric environment. The conjugation of 5'-biotin-aptamer and AuNP-SA resulted in a 2.6 nm increase in HD that was much smaller than that of AuNP-PEG-SA. It was believed that the extra PEGylation and COOH-NH_2 conjugation would lead to different SA coverage and orientation on the AuNP surface compared to direct adsorption. These differences resulted in different surface properties, which further affected the secondary structure of the aptamer and its stretching extent. The conformational change of proteins adsorbed to AuNP[38] was also responsible for the change in reactivity with other molecules, for example, the SA-biotin reaction.

3.4 Conclusion

AuNPs were functionalized with a DNA aptamer against H3N2 influenza virus via PEGylation and adsorption. PEG and SA coating of AuNPs induced changes of the local dielectric environment, which resulted in a redshift of the LSPR band. Beyond coating with the first layer (PEG or SA), further modification did not induce any additional changes in the LSPR band. The HDs of each intermediate and final product increased in either method, indicating successful modification.

3.5 References

(1) Jans, H.; Huo, Q. *Chemical Society Reviews* **2012**, *41*, 2849.

(2) Saha, K.; Agasti, S. S.; Kim, C.; Li, X.; Rotello, V. M. *Chemical Reviews* **2012**, *112*, 2739.

(3) Wilson, R. *Chemical Society Reviews* **2008**, *37*, 2028.

(4) Elghanian, R.; Storhoff, J. J.; Mucic, R. C.; Letsinger, R. L.; Mirkin, C. A. *Science* **1997**, *277*, 1078.

(5) Storhoff, J. J.; Lazarides, A. A.; Mucic, R. C.; Mirkin, C. A.; Letsinger, R. L.; Schatz, G. C. *Journal of the American Chemical Society* **2000**, *122*, 4640.

(6) Rechberger, W.; Hohenau, A.; Leitner, A.; Krenn, J. R.; Lamprecht, B.; Aussenegg, F. R. *Optics Communications* **2003**, *220*, 137.

(7) Daniel, M.-C.; Astruc, D. *Chemical Reviews* **2004**, *104*, 293.

(8) Kelly, K. L.; Coronado, E.; Zhao, L. L.; Schatz, G. C. *The Journal of Physical Chemistry B* **2003**, *107*, 668.

(9) Nehl, C. L.; Liao, H.; Hafner, J. H. *Nano Letters* **2006**, *6*, 683.

(10) Katz, E.; Willner, I. *Angewandte Chemie International Edition* **2004**, *43*, 6042.

(11) Mout, R.; Moyano, D. F.; Rana, S.; Rotello, V. M. *Chemical Society Reviews* **2012**, *41*, 2539.

(12) Sperling, R. A.; Parak, W. J. *Surface modification, functionalization and bioconjugation of colloidal inorganic nanoparticles*, 2010; Vol. 368.

(13) Liu, J.; Lu, Y. *Journal of the American Chemical Society* **2003**, *125*, 6642.

(14) Li, H.; Rothberg, L. *Proceedings of the National Academy of Sciences of the United States of America* **2004**, *101*, 14036.

(15) Lee, J.-S.; Han, M. S.; Mirkin, C. A. *Angewandte Chemie* **2007**, *119*, 4171.

(16) Kneipp, K.; Wang, Y.; Kneipp, H.; Perelman, L. T.; Itzkan, I.; Dasari, R. R.; Feld, M. S. *Physical Review Letters* **1997**, *78*, 1667.

(17) Nie, S.; Emory, S. R. *Science* **1997**, *275*, 1102.

(18) Wang, Y.; Yan, B.; Chen, L. *Chemical Reviews* **2013**, *113*, 1391.

(19) Qian, X.; Peng, X.-H.; Ansari, D. O.; Yin-Goen, Q.; Chen, G. Z.; Shin, D. M.; Yang, L.; Young, A. N.; Wang, M. D.; Nie, S. *Nat Biotech* **2008**, *26*, 83.

(20) Driskell, J. D.; Jones, C. A.; Tompkins, S. M.; Tripp, R. A. *Analyst* **2011**, *136*, 3083.

(21) Storhoff, J. J.; Lucas, A. D.; Garimella, V.; Bao, Y. P.; Muller, U. R. *Nat Biotech* **2004**, *22*, 883.

(22) Hermann, T.; Patel, D. J. *Science* **2000**, *287*, 820.

(23) Tan, W.; Donovan, M. J.; Jiang, J. *Chemical Reviews* **2013**, *113*, 2842.

(24) Kim, Y. S.; Kim, J. H.; Kim, I. A.; Lee, S. J.; Jurng, J.; Gu, M. B. *Biosensors and Bioelectronics* **2010**, *26*, 1644.

(25) Guo, S.; Du, Y.; Yang, X.; Dong, S.; Wang, E. *Analytical Chemistry* **2011**, *83*, 8035.

(26) Wei, H.; Li, B.; Li, J.; Wang, E.; Dong, S. *Chemical Communications* **2007**, 3735.

(27) Deng, C.; Chen, J.; Nie, Z.; Wang, M.; Chu, X.; Chen, X.; Xiao, X.; Lei, C.; Yao, S. *Analytical Chemistry* **2009**, *81*, 739.

(28) Torres-Chavolla, E.; Alocilja, E. C. *Biosensors and Bioelectronics* **2009**, *24*, 3175.

(29) Yuan, J.; Wu, S.; Duan, N.; Ma, X.; Xia, Y.; Chen, J.; Ding, Z.; Wang, Z. *Talanta* **2014**, *127*, 163.

(30) Wongphatcharachai, M.; Wang, P.; Enomoto, S.; Webby, R. J.; Gramer, M. R.; Amonsin, A.; Sreevatsan, S. *Journal of Clinical Microbiology* **2013**, *51*, 46.

(31) Brown, K. R.; Walter, D. G.; Natan, M. J. *Chem Mater* **2000**, *12*, 306.

(32) Frens, G. *Nature* **1973**, *241*, 20.

(33) Leng, W.; Vikesland, P. J. *Langmuir* **2014**, *30*, 8342.

(34) Willets, K. A.; Van Duyne, R. P. *Annual Review of Physical Chemistry* **2007**, *58*, 267.

(35) Hendrickson, W. A.; Pähler, A.; Smith, J. L.; Satow, Y.; Merritt, E. A.; Phizackerley, R. P. *Proceedings of the National Academy of Sciences* **1989**, *86*, 2190.

(36) Brewer, S. H.; Glomm, W. R.; Johnson, M. C.; Knag, M. K.; Franzen, S. *Langmuir* **2005**, *21*, 9303.

(37) Cañaveras, F.; Madueño, R.; Sevilla, J. M.; Blázquez, M.; Pineda, T. *The Journal of Physical Chemistry C* **2012**, *116*, 10430.

(38) Shang, L.; Wang, Y.; Jiang, J.; Dong, S. *Langmuir* **2007**, *23*, 2714.

3.6 Figures

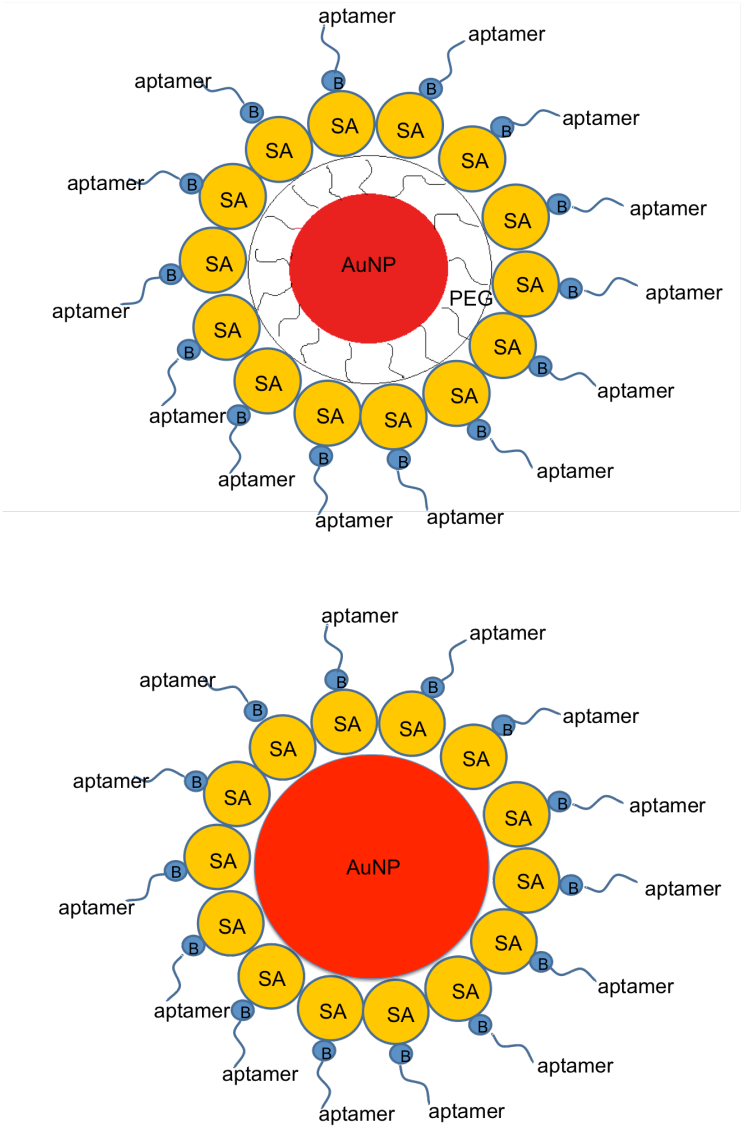

Figure 3-1. Top: Cartoon of AuNP functionalization via PEGylation; Bottom: Cartoon of AuNP functionalization via adsorption. SA is streptavidin, and B is biotin.

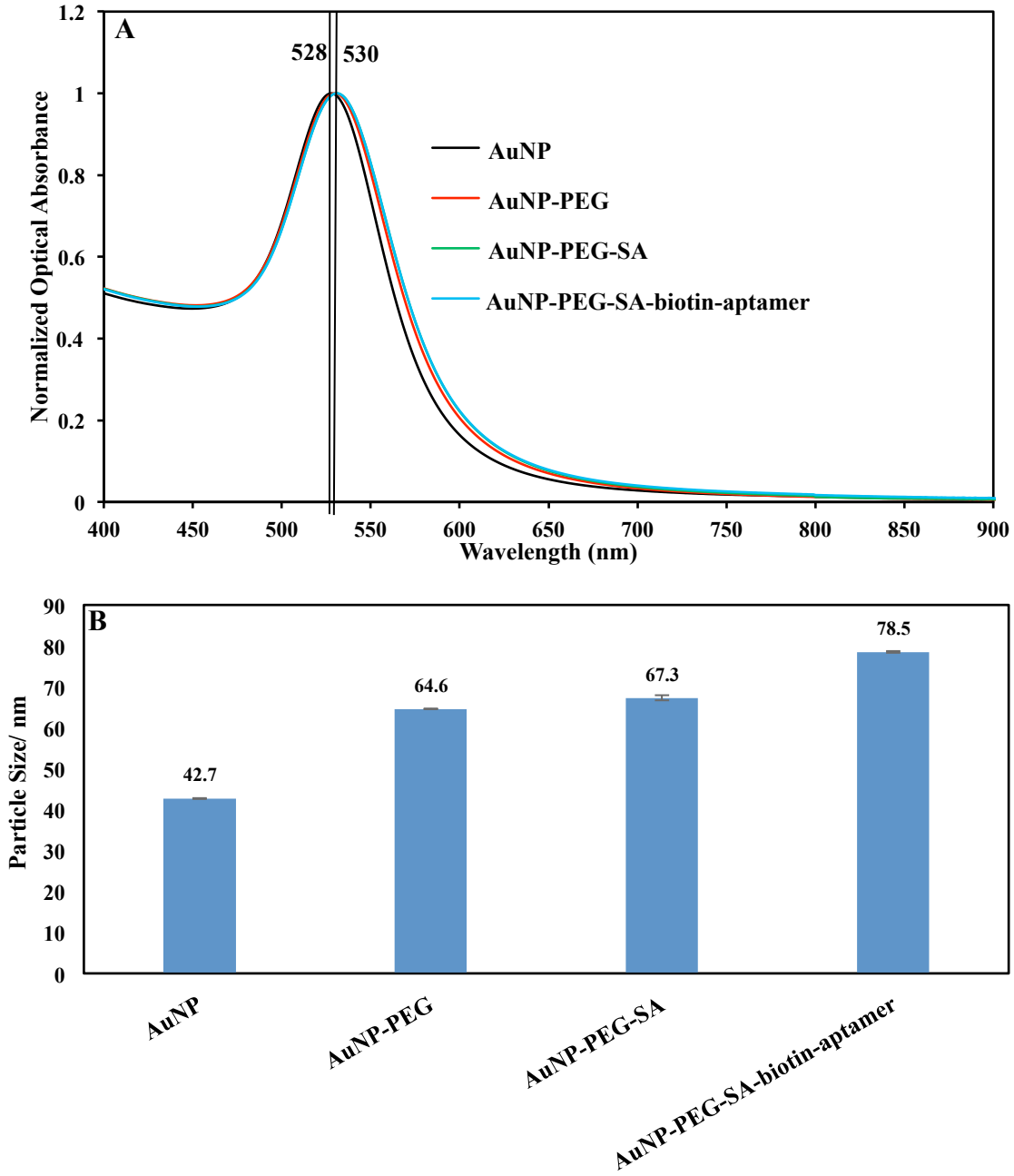

Figure 3-2. (A) UV-vis spectra of original AuNP, AuNP-PEG, AuNP-PEG-SA, and AuNP-PEG-SA-biotin-aptamer. The LSPR of AuNP peaks at 528 nm while the LSPR of other intermediate and final products peak at 530 nm. (B) Particle size of original AuNP, AuNP-PEG, AuNP-PEG-SA, and AuNP-PEG-SA-biotin-aptamer.

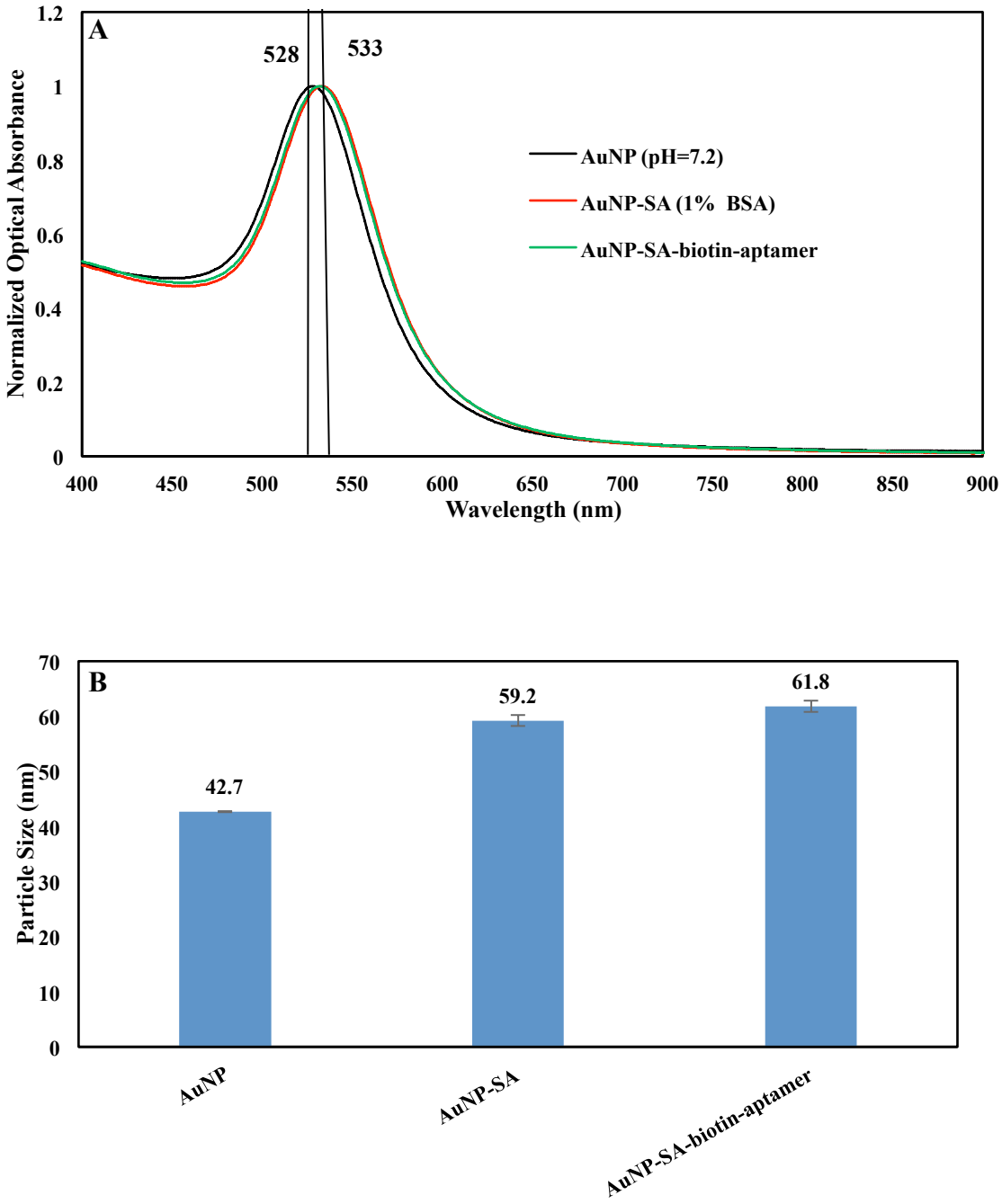

Figure 3-3. (A) UV-vis spectra of AuNP, AuNP-SA, and AuNP-SA-biotin-aptamer. The LSPR of AuNP peaks at 528 nm while the LSPR of AuNP-SA and AuNP-SA-biotin-aptamer peaks at 533 nm. (B) Particle size of original AuNP, AuNP-SA, and AuNP-SA-biotin-aptamer.

Chapter 4. Conclusion

4.1 High-purity Gold Nano-clusters as SERS Substrate

We developed a simple method to reproducibly isolate PEGylated AuNP nano-clusters for use as an ultrasensitive SERS substrate. Density gradient centrifugation was applied to a population of heterogeneous aggregates. Monomers, small nano-clusters (2-4 nanospheres), and large nano-clusters (>5 nanospheres) were separated in three distinct bands. We confirmed that the Raman signal from MGITC could be clearly recorded from a single nano-cluster. Absent the non-active monomers, the high-purity nano-clusters hold promising potential in developing ultrasensitive SERS tags for bio-imaging and biosensor applications.

4.2 Functionalization of Gold Nanoparticle with Aptamers

In order to develop a biosensor for flu virus, we functionalized AuNPs with aptamers against swine influenza H3N2 viruses through two distinct methods. Both methods start with preparation of AuNP-streptavidin and take advantage of the strong streptavidin-biotin reaction to conjugate biotin-modified aptamers. The first method was accomplished via AuNP PEGylation followed by covalent conjugation with streptavidin, while the second method was achieved simply by self-assembly of streptavidin on AuNP. PEG and SA that directly coated the surface of AuNPs surface induced changes in the local dielectric environment, which resulted in a redshift of the LSPR band. Beyond coating with the first layer (PEG or SA), further modification did not induce any additional changes in the LSPR band. The hydrodynamic diameter of each intermediate and final product increased in either method, indicating successful modification.

4.3 Possible Future Work

Future work may include but is not limited to the combination of chapter 2 and chapter 3. In other words, the modification of aptamers to nano-cluster based SERS substrates can lead to detection of influenza virus with high sensitivity and specificity. Since the non-active monomers can be removed from a population of nano-clusters, type I error is ruled out. The detection limit will be significantly improved compared to those methods using AuNP aggregates containing a considerable amount of non-active monomers.

Appendix

Functionalization of Multi-walled Carbon Nanotubes with Lipid Bilayer

A.1 Introduction

Supported lipid bilayers (SLB) on a solid substrate surface, developed by Tamm[1] and McConnell[2], provide a robust artificial cell membrane in a controllable manner. Taking advantage of the unique physicochemical properties of nanomaterials, lipid-nanostructure hybrids have attracted enormous interest in a wide range of applications[3] including drug delivery[4,5], cancer therapy[6], biosensor[7,8], and cell mimicking[9]. Carbon nanotubes (CNTs) possess unique electrochemical properties for chemical[10] and biological sensing[11]. Recent advances in SLB-CNT hybrids have exhibited promising potential for cell activity monitoring[12,13] and photo-switchable devices[14]. For example, Zhou et al.[12] developed a biosensor to detect single ion channel activity of SLB via a CNT field effect transistor.

Hydrophilic nanomaterials such as silicon nanowire[15,16], silicon nanobead[17,18], and gold nanoparticles[19] readily provide a hydrophilic substrate for SLB attachment, rupture, and diffusion[18]. Unlike hydrophilic nanomaterials, CNTs interact with amphiphilic lipid molecules via hydrophobic interactions, which lead to the formation of a lipid monolayer[20]. To address this challenge, several routes have been proposed to modify the CNT surface for SLB formation. He[21] and Dayani[22] fabricated SLB-CNT hybrids via covalent modification, in which –COOH groups were firstly introduced via oxidation, followed by chemical conjugation between –COOH groups on oxidized CNTs and $–NH_2$ groups on lipid. An alternative approach was suggested by Artyukhin et al.[23], in which single-walled carbon nanotubes (SWCNTs) suspended on TEM grids were modified with

hydrophilic polymer layers, and then a continuous lipid bilayer shell was self-assembled around this structure.

In this study, we modified multi-walled carbon nanotubes (MWCNTs) with lipid bilayers in an aqueous solution. SLB-MWCNT hybrids were fabricated in a two-step manner. MWCNTs were firstly suspended in water via sonication in the aid of sodium poly(styrenesulphonate) (PSS). Lipid bilayers were then self-assembled on the hydrophilic surface of PSS-MWCNTs. The modified MWCNTs were intended to serve as abiotic surrogates for Ebola virus in studies of fate and transport of the virus in the environment.

A.2 Materials and Methods

A.2.1 Reagents and Materials

MWCNTs were purchased from Nanostructured and Amorphous Materials (Houston, TX, USA). The characterization information reported by the manufacturer is listed in Table 1. 1,2-dioleoyl-3-trimethylammonium-propane (DOTAP) was obtained from Avanti Polar Lipids (Alabaster, AL, USA). Texas Red 1,2-dihexadecanoyl-sn-glycero-3-phosphoethanolamine, triethylammonium salt (Texas Red-DHPE) was purchased from Life Technologies (Grand Island, NY, USA). Both lipids were received as chloroform solution. Sodium poly(styrenesulphonate) (PSS) and poly(dimethyldiallylammonium chloride) (PDDA) were obtained from Sigma Aldrich (St. Louis, MO, USA). All reagents were used as received without further treatment.

A.2.2 Suspension of PSS-MWCNTs

12 mg of MWCNT powder was immersed into 100 mL of 1% PSS solution. The mixture was then sonicated for 30 min. Excess PSS was removed via four rounds of

centrifugation (12000 g × 10 min) and re-suspensed in deionized water. The final concentration of the MWCNT suspension was brought to 0.24 g/L.

Atomic force microscopy (AFM) images were captured using a Nanoscope III (Digital Instruments/Veeco Metrology Group, USA). Briefly, a clean mica substrate was dipped into 1% PDDA solution for 10 min to make it a uniformly charged surface[24]. Loosely bound PDDA was washed by thorough rinsing with DI water. The charged mica substrate was then drop-coated with 3 μL of PSS-MWCNT suspension and left to dry for 30 min, followed by AFM imaging.

A.2.3 Preparation of Liposomes

A published method was followed to prepare liposomes[25]. Briefly, DOTAP and Texas Red-DHPE (TR-DHPE) were mixed thoroughly in a glass vial at a ratio of 50:1. Lipids were dried under an argon stream for 1 hour and then left under vacuum for 2 hours to remove the solvent residues. The dried lipids were hydrated with deionized water to obtain a final concentration of 2 mg/mL and shaken for 1 hour. The hydrated lipids were extruded 30 times through a 50 nm polycarbonate membrane using an Avanti mini extruder (Avanti Polar Lipids, Inc.). The liposome solution was stored at 4 °C.

A.2.4 Fabrication of SLB-MWCNT Hybrids

0.5 mL of PSS-MWCNT suspension (0.24 g/L) was mixed with 0.5 mL of liposome solution (2 mg/mL). The mixture was incubated overnight for complete SLB formation on MWCNTs. Excess liposomes were removed via three rounds of centrifugation (12000 g × 10 min) and re-suspension in 1 mL of deionized water. The total fluorescence of the washed SLB-MWCNT suspension was measured. The zeta potential of the washed PSS-

MWCNT and SLB-MWCNT was recorded using a Zetasizer NanoZS instrument (Malvern Instruments, UK).

A.3 Results and Discussion

With the aid of PSS, sonication helped to disperse and stabilize the majority of MWCNTs into individual nanotubes[24,26-29] (Figure A-1). The diameter of suspended PSS-MWCNTs was 61 ± 23 nm while the length was 871 ± 535 nm, which matches the characterization information reported by the manufacturer.

As PSS is a poly-anion composed of many sulphonate groups, the modification of MWCNTs with PSS turned the surface of MWCNTs highly hydrophilic and negatively charged[23]. The electrostatic interaction between the negatively charged MWCNTs and positively charged liposome composed of DOTAP triggered the self-assembly of SLB on the MWCNT surface[23]. A similar strategy was also adopted by Moya et al. for the lipid coating on polyelectrolyte capsules[30]. The SLB formation on PSS-MWCNTs resulted in charge reversal indicated by the change of zeta potential from -57 mV to + 61 mV (Figure A-2). However, no fluorescence was detected for the TR-DHPE in the DOTAP (2% TR-DHPE)-PSS-MWCNT suspension (Figure A-3), which contradicted the results of Moya[30]'s, Artyukhin[23]'s, and Dayani[22]'s studies. The difference in CNT diameter and length, as well as the fluorescent dye species may contribute to the different results observed in this study and others' researches. One possible cause was fluorescence quenching by MWCNTs[31]. The absorption spectra of CNTs span a wide range of wavelengths[29,32] and overlap the photoluminescence spectra of various fluorophores[31]. The fluorescent emission of Texas Red-DHPE might be quenched by MWCNTs.

A.4 Conclusion

SLB-MWCNTs were fabricated via the electrostatic interaction between positively charged DOTAP liposome and negatively charged PSS-MWCNTs. A change in the sign of zeta potential indicated the self-assembly of SLB on MWCNT surface. However, the absence of a fluorescent signal from DOTAP (2% TR-DHPE)-PSS-MWCNT contradicted the conclusion of SLB formation on MWCNTs. Fluorescence quenching might be one possible cause for these contradictory phenomena. Future work on elucidating the possible fluorescence quenching may be expected to clearly address this problem.

A.5 References

(1) Tamm, L. K.; McConnell, H. M. *Biophysical Journal* **1985**, *47*, 105.

(2) Brian, A. A.; McConnell, H. M. *Proceedings of the National Academy of Sciences* **1984**, *81*, 6159.

(3) Lee, Y. K.; Lee, H.; Nam, J.-M. *NPG Asia Mater* **2013**, *5*, e48.

(4) Liu, J.; Jiang, X.; Ashley, C.; Brinker, C. J. *Journal of the American Chemical Society* **2009**, *131*, 7567.

(5) Mackowiak, S. A.; Schmidt, A.; Weiss, V.; Argyo, C.; von Schirnding, C.; Bein, T.; Bräuchle, C. *Nano Letters* **2013**, *13*, 2576.

(6) Wang, D.; Huang, J.; Wang, X.; Yu, Y.; Zhang, H.; Chen, Y.; Liu, J.; Sun, Z.; Zou, H.; Sun, D.; Zhou, G.; Zhang, G.; Lu, Y.; Zhong, Y. *Biomaterials* **2013**, *34*, 7662.

(7) Baciu, C. L.; Becker, J.; Janshoff, A.; Sönnichsen, C. *Nano Letters* **2008**, *8*, 1724.

(8) Galush, W. J.; Shelby, S. A.; Mulvihill, M. J.; Tao, A.; Yang, P.; Groves, J. T. *Nano Letters* **2009**, *9*, 2077.

(9) Mossman, K. D.; Campi, G.; Groves, J. T.; Dustin, M. L. *Science* **2005**, *310*, 1191.

(10) Kong, J.; Franklin, N. R.; Zhou, C.; Chapline, M. G.; Peng, S.; Cho, K.; Dai, H. *Science* **2000**, *287*, 622.

(11) Star, A.; Gabriel, J.-C. P.; Bradley, K.; Grüner, G. *Nano Letters* **2003**, *3*, 459.

(12) Zhou, W. *Scientific Report* **2015**, *5*, 9208.

(13) Liu, L.; Yang, C.; Zhao, K.; Li, J.; Wu, H.-C. *Nat Commun* **2013**, *4*.

(14) Ye, J.-S.; Cui, H.-F.; Wen, Y.; Zhang, W. D.; Ottova, A.; Tien, H. T.; Xu, G. Q.; Sheu, F.-S. *Electrochemistry Communications* **2005**, *7*, 81.

(15) Martinez, J. A.; Misra, N.; Wang, Y.; Stroeve, P.; Grigoropoulos, C. P.; Noy, A. *Nano Letters* **2009**, *9*, 1121.

(16) Huang, S.-C. J.; Artyukhin, A. B.; Martinez, J. A.; Sirbuly, D. J.; Wang, Y.; Ju, J.-W.; Stroeve, P.; Noy, A. *Nano Letters* **2007**, *7*, 3355.

(17) Savarala, S.; Ahmed, S.; Ilies, M. A.; Wunder, S. L. *Langmuir* **2010**, *26*, 12081.

(18) Mornet, S.; Lambert, O.; Duguet, E.; Brisson, A. *Nano Letters* **2005**, *5*, 281.

(19) Zhang, L.; Sun, X.; Song, Y.; Jiang, X.; Dong, S.; Wang, E. *Langmuir* **2006**, *22*, 2838.

(20) Li, Q.; Renneckar, S. *Biomacromolecules* **2011**, *12*, 650.

(21) He, P.; Urban, M. W. *Biomacromolecules* **2005**, *6*, 2455.

(22) Dayani, Y.; Malmstadt, N. *Langmuir* **2012**, *28*, 8174.

(23) Artyukhin, A. B.; Shestakov, A.; Harper, J.; Bakajin, O.; Stroeve, P.; Noy, A. *Journal of the American Chemical Society* **2005**, *127*, 7538.

(24) Sinani, V. A.; Gheith, M. K.; Yaroslavov, A. A.; Rakhnyanskaya, A. A.; Sun, K.; Mamedov, A. A.; Wicksted, J. P.; Kotov, N. A. *Journal of the American Chemical Society* **2005**, *127*, 3463.

(25) Afanasenkau, D.; Offenhäusser, A. *Langmuir* **2012**, *28*, 13387.

(26) O'Connell, M. J.; Boul, P.; Ericson, L. M.; Huffman, C.; Wang, Y.; Haroz, E.; Kuper, C.; Tour, J.; Ausman, K. D.; Smalley, R. E. *Chemical Physics Letters* **2001**, *342*, 265.

(27) Islam, M. F.; Rojas, E.; Bergey, D. M.; Johnson, A. T.; Yodh, A. G. *Nano Letters* **2003**, *3*, 269.

(28) Moore, V. C.; Strano, M. S.; Haroz, E. H.; Hauge, R. H.; Smalley, R. E.; Schmidt, J.; Talmon, Y. *Nano Letters* **2003**, *3*, 1379.

(29) Yu, J.; Grossiord, N.; Koning, C. E.; Loos, J. *Carbon* **2007**, *45*, 618.

(30) Moya, S.; Donath, E.; Sukhorukov, G. B.; Auch, M.; Bäumler, H.; Lichtenfeld, H.; Möhwald, H. *Macromolecules* **2000**, *33*, 4538.

(31) Zhu, Z.; Yang, R.; You, M.; Zhang, X.; Wu, Y.; Tan, W. *Anal Bioanal Chem* **2010**, *396*, 73.

(32) Bachilo, S. M.; Strano, M. S.; Kittrell, C.; Hauge, R. H.; Smalley, R. E.; Weisman, R. B. *Science* **2002**, *298*, 2361.

(33) Brewer, S. H.; Glomm, W. R.; Johnson, M. C.; Knag, M. K.; Franzen, S. *Langmuir* **2005**, *21*, 9303.

A.6 Tables and Figures

Table A-1. Characterization information of MWCNTs reported by manufacturer.	
Purity	95%
Outside Diameter (OD)	50~80 nm
Inside Diameter (ID)	5~15 nm
Length	0.5~2 μm
Surface Area	40 m^2/g
Color	Black

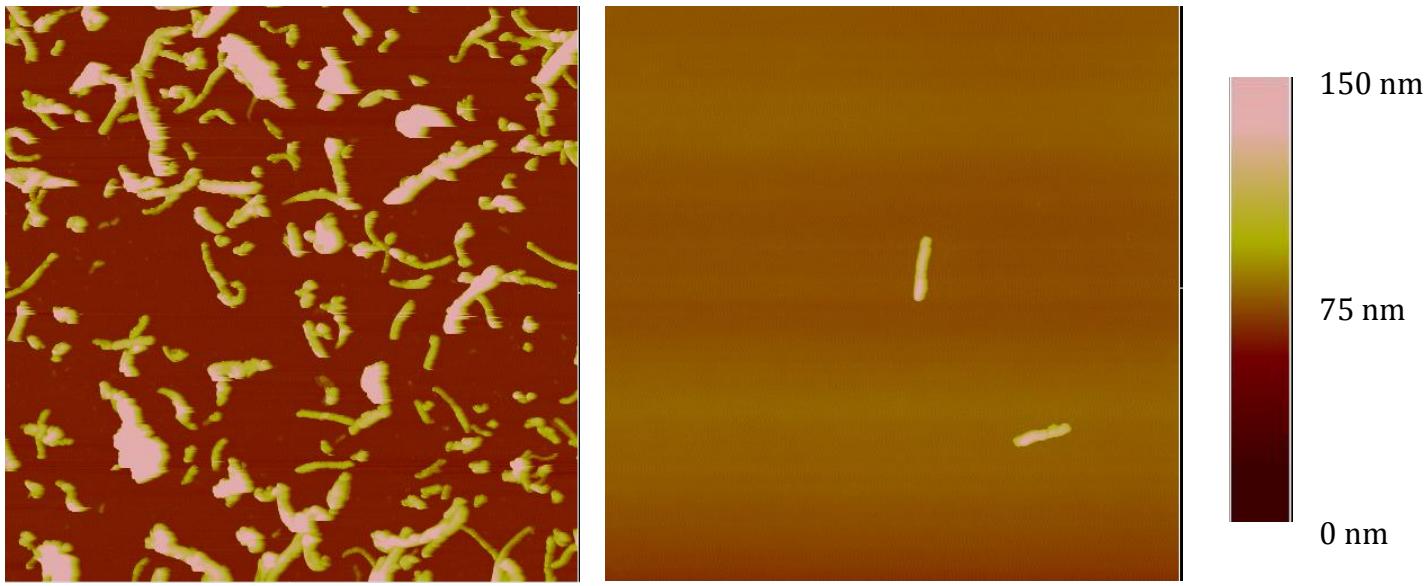

Figure A-1. AFM images of PSS-MWCNTs. Image scale: 5 μm × 5 μm.

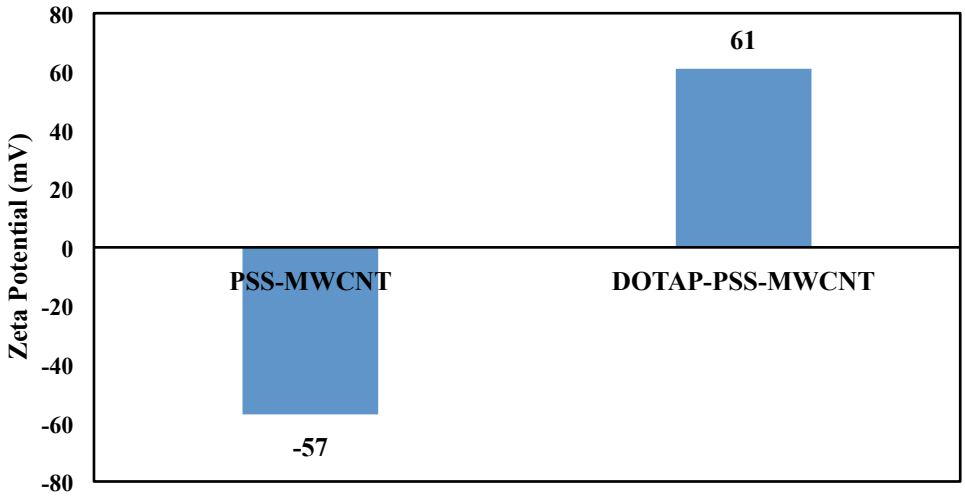

Figure A-2. Zeta potential of PSS-MWCNT and DOTAP-PSS-MWCNT suspensions.

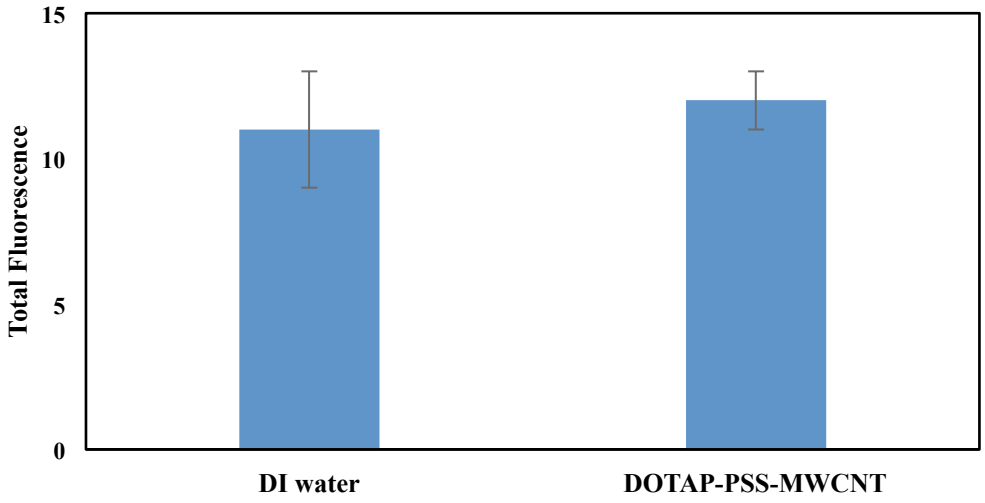

Figure A-3. Total fluorescence of DI water and DOTAP-PSS-MWCNT.